ARTICLE

https://doi.org/10.1038/s41586-019-0889-9

Global environmental consequences of twenty-first-century ice-sheet melt

Nicholas R. Golledge[1,2]*, Elizabeth D. Keller[2], Natalya Gomez[3], Kaitlin A. Naughten[4], Jorge Bernales[5], Luke D. Trusel[6] & Tamsin L. Edwards[7]

Government policies currently commit us to surface warming of three to four degrees Celsius above pre-industrial levels by 2100, which will lead to enhanced ice-sheet melt. Ice-sheet discharge was not explicitly included in Coupled Model Intercomparison Project phase 5, so effects on climate from this melt are not currently captured in the simulations most commonly used to inform governmental policy. Here we show, using simulations of the Greenland and Antarctic ice sheets constrained by satellite-based measurements of recent changes in ice mass, that increasing meltwater from Greenland will lead to substantial slowing of the Atlantic overturning circulation, and that meltwater from Antarctica will trap warm water below the sea surface, creating a positive feedback that increases Antarctic ice loss. In our simulations, future ice-sheet melt enhances global temperature variability and contributes up to 25 centimetres to sea level by 2100. However, uncertainties in the way in which future changes in ice dynamics are modelled remain, underlining the need for continued observations and comprehensive multi-model assessments.

Mass loss from the Antarctic[1,2] and Greenland[2,3] ice sheets and from mountain glaciers[4] is accelerating[5], primarily as a consequence of rising atmospheric and oceanic temperatures. This ice loss contributes to the recently observed acceleration in global-mean sea-level rise[6] and may also be linked to weakening of the Atlantic Meridional Overturning Circulation (AMOC)[7,8]. It is likely that global temperatures in the year 2100 will exceed the 2 °C target set by the Paris Agreement[9], because simulations indicate a likely increase of 2.6–4.0 °C above pre-industrial baseline temperatures even if the pledges made by signatory countries of the Paris Agreement are honoured (see https://climateactiontracker.org/). The Greenland Ice Sheet, the West Antarctic Ice Sheet and the AMOC are all capable of abrupt changes under perturbed climate conditions[10]. Recent research suggests that tipping points in parts of the West Antarctic Ice Sheet may have already been passed[11,12]. Coastal flooding events in low-latitude areas will probably double in frequency by 2050 if sea-level rise reaches 0.1–0.2 m above present[13], with less-developed small island nations likely to experience the greatest local climate changes if the Paris targets are not met[14]. The consequences of predicted future changes in the Earth system will therefore be societally and economically important, but will be spatially variable, and the spread of future sea-level-rise scenarios remains large owing to uncertainties in the processes that are likely to control future ice-sheet retreat[15]. Even within climatologies that are consistent with the Paris targets there is a likelihood of at least 0.5 m of global-mean sea-level rise by 2100[16].

Global-mean sea level depends primarily on five key contributors: the Greenland and Antarctic ice sheets, mountain glaciers, land water storage and ocean thermal expansion. Of these, the ice-sheet components represent the greatest sea-level potential and are the most capable of abrupt or nonlinear change. Previous scenario-based simulations using dynamical ice-sheet models and forced by climate scenarios adopted by the Intergovernmental Panel on Climate Change (IPCC) forecast a range of possible sea-level contributions by the end of the century[17–20]. However, so far, no single study has simulated both the Greenland and Antarctic ice sheets at high resolution and in a consistent framework that incorporates time-varying multi-parameter mass-balance constraints from satellite-era observational records.

Furthermore, experiments undertaken for Coupled Model Intercomparison Project phase 5 (CMIP5) did not include explicit representation of future ice-sheet discharge[21–23]. This means that the climate simulations most commonly used to inform global policy decisions currently do not account for ice–ocean–atmosphere feedbacks that may arise as a consequence of ice-sheet melting.

Experimental methods and approach

Here we present scenario-based simulations of the Greenland and Antarctic ice sheets at horizontal resolutions of 2.5 km and 5 km respectively. We use a sub-grid-scale grounding-line parameterization and a hybrid stress-balance calculation that simultaneously solves flow equations that capture the dynamics of inland ice flow, ice streams and ice shelves[24]. We drive these experiments with spatially and temporally varying monthly and annual climatologies from multi-model ensemble-mean outputs of CMIP5, for the period 1860–2100. Our coupled ice-sheet–ice-shelf model uses a calculation of basal melt rate derived from the inversion of present-day melt rates[25] (Methods), which allows spatially distributed sub-ice-shelf melt to be captured realistically. To investigate the consequences of incorporating previously ignored ice–ocean–atmosphere feedbacks, we include offline coupling between our ice-sheet model and an intermediate-complexity climate model with a fully coupled ocean and atmosphere, passing results from one to the other in a series of iterations.

Results and key findings

Observation-constrained ice-sheet simulations

Figure 1 illustrates the time evolution of our two simulated ice sheets in the first iteration. We compare modelled quantities of net mass balance, surface mass balance, basal melt of ice shelves and dynamic (calving) losses against empirical constraints from 23 independent studies whose records collectively span the period 1900–2017, with the most complete coverage occurring since 1980. Although we are not able to constrain

[1]Antarctic Research Centre, Victoria University of Wellington, Wellington, New Zealand. [2]GNS Science, Lower Hutt, New Zealand. [3]Earth and Planetary Sciences, McGill University, Montreal, Quebec, Canada. [4]British Antarctic Survey, Cambridge, UK. [5]MARUM Centre for Marine Environmental Sciences, University of Bremen, Bremen, Germany. [6]Department of Geology, Rowan University, Glassboro, NJ, USA. [7]Department of Geography, Kings College, London, UK. *e-mail: nicholas.golledge@vuw.ac.nz

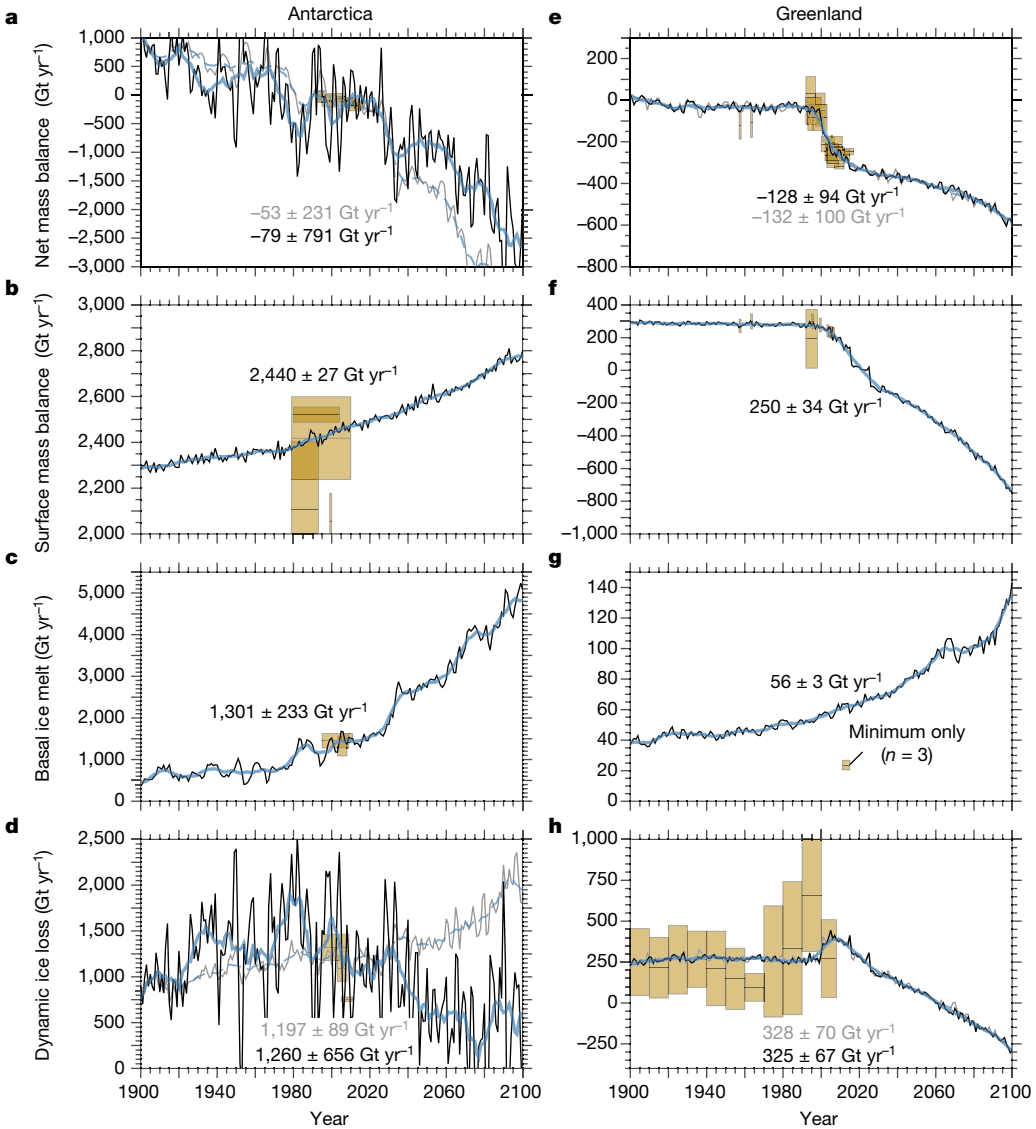

Fig. 1 | Simulated and observed ice-sheet mass balance. a–d, Numerical ice-sheet simulation of net mass balance (**a**), surface mass balance (**b**), basal ice melt (**c**) and dynamic (calving) mass loss (**d**) for the Antarctic Ice Sheet. **e–h**, As in **a–d**, but for the Greenland Ice Sheet. Negative dynamic losses (**h**) imply thickening. Forcing scenario is RCP8.5; experiments do not include meltwater feedback. Gold boxes show the time span (*x* axis) and uncertainty (*y* axis) of empirical data values used as targets during parameter optimization, from sources detailed in Extended Data Tables 1 and 2. Circum-Greenland basal melting is constrained by only one assessment from three glaciers; Greenland calving constraints (**h**) are from data-constrained modelling (Extended Data Table 2). Black lines show annual mass changes for grounded ice only, with the 10-yr running mean shown in blue. Grey lines show mass changes for the entire ice sheet, including ice shelves, with the 10-yr running mean shown by the dashed blue line. In **a**, **d**, **e** and **h**, black text denotes the 1990–2010 mean for grounded ice and grey text denotes the 1990–2010 mean for grounded and floating ice; uncertainties indicate one standard deviation of the 1990–2010 model range.

all parameters throughout this entire period, and acknowledging that uncertainties in these quantities are high in some cases (Fig. 1b), our optimized model parameterization (Methods) allows a close fit to be achieved in nearly all cases.

Using this parameterization we run a suite of simulations of future ice sheets in which we impose climatologies from Representative Concentration Pathway (RCP) 4.5 and 8.5 scenarios. Previous studies have shown that ice–ocean interactions—which are not captured in CMIP5 simulations—substantially affect ice-sheet evolution[26] and far-field changes in climate[27]. This occurs primarily as a consequence of a decadal- to centennial-scale buoyancy-induced reduction in high-latitude ocean overturning when ice-sheet melt forms a freshwater lens over the surface of the ice-sheet proximal ocean. By stratifying the water column, upwelling warm water does not mix with colder surface layers, essentially trapping heat in the subsurface where it can spread laterally and increase melting at glacial grounding lines[28,29]. Our coarse-resolution ocean model might underestimate effects from short-term variability in mixed-layer thickness, which might also influence ocean temperatures (Methods). We introduce annual transient freshwater fluxes from our simulated ice sheets into the climate simulations from 2000 to 2100 under RCP4.5 and RCP8.5 conditions. Time-evolving fluxes are calculated by assuming that all mass changes in the ice sheet result in net fluxes of freshwater to the proximal ocean, which by 2100 reach maxima of approximately 0.042 Sv and 0.015 Sv for Antarctica and Greenland, respectively, under RCP4.5, and 0.160 Sv and 0.018 Sv under RCP 8.5. We add anomalies in subsurface ocean temperature, surface air temperature and precipitation that arise as a consequence of this meltwater addition (compared to a control with no meltwater addition) to the previously used CMIP5 fields and repeat the ice-sheet simulations.

Future ice-sheet changes and contribution to sea level

In Fig. 2 we present the modelled sea-level contributions from the two ice sheets by 2100, under RCP4.5 and RCP8.5 conditions, with

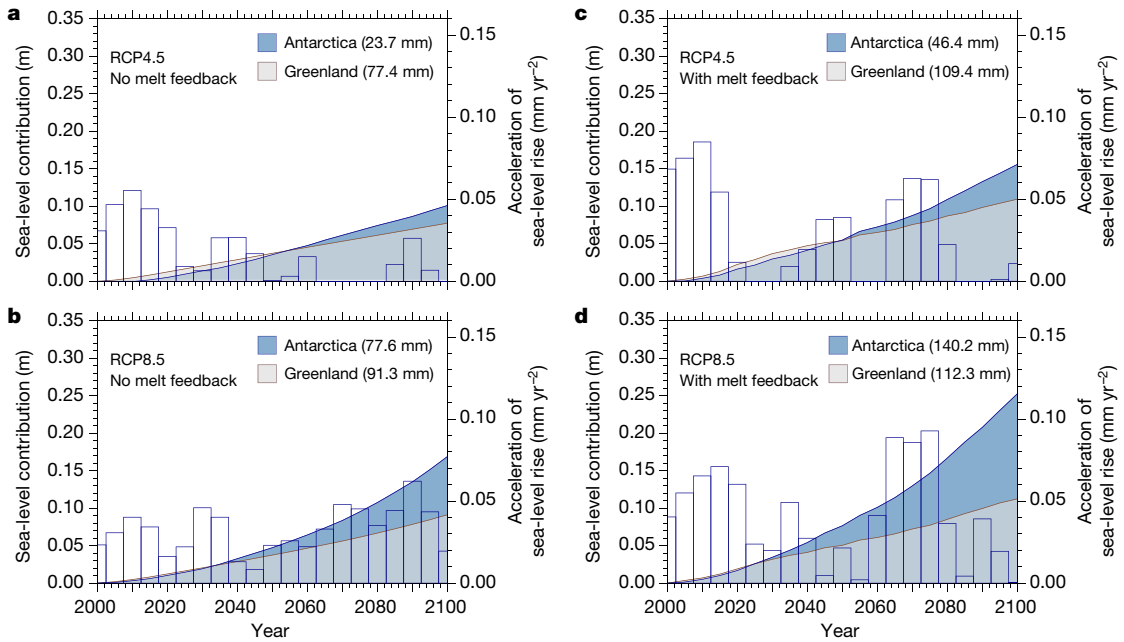

Fig. 2 | Sea-level contributions from Greenland and Antarctica. Predictions of cumulative sea-level-equivalent mass loss (curves and shading; left-hand axis) from the Greenland and Antarctic ice sheets to 2100 under RCP4.5 (**a**, **c**) and RCP8.5 (**b**, **d**) climate trajectories, without (**a**, **b**) and with (**c**, **d**) meltwater feedback. The numbers in parentheses in each legend give the individual sea-level contributions at 2100. Histograms show the rates of acceleration of sea-level rise (positive only, right-hand axis) based on the combined total of Antarctic and Greenland contributions. Red lines show Greenland contribution. Blue lines show combined ice sheet total. Intersections occur when Antarctic accumulation partly offsets Greenland loss.

and without ice–ocean–atmosphere feedbacks. It is clear from these trajectories that the sea-level contribution from the Greenland Ice Sheet is approximately linear with time, increasing in magnitude with stronger forcing. The response of the Antarctic Ice Sheet is slower in the first decades of the century and subsequently accelerates. Combining these two sources yields a globally averaged pattern of sea-level rise that exhibits episodic accelerations during the century, with the fastest increase in the rate of sea-level rise occurring during the period 2065–2075 under RCP8.5 with melt feedback incorporated (Fig. 2d).

Simulated changes in ice-sheet geometries by 2100 under RCP8.5 with ice–ocean–atmosphere feedbacks incorporated show that in Antarctica (Fig. 3a) the greatest thickness changes this century occur in the grounded ice of the Amundsen Sea sector of West Antarctica. This is associated with substantial recession of the Thwaites Glacier and neighbouring Pine Island Glacier. Considerable thinning of all the major ice shelves and the collapse of Larsen C and many of the Dronning Maud Land ice shelves is also evident. In Greenland (Fig. 3b) the largest thickness changes take place along the southeast and northwest margins of the ice sheet, with thinning also occurring along lower portions of the Northeast Greenland Ice Stream. To estimate the relative importance of different mass-balance components in controlling future evolution of each ice sheet, we compare basin-integrated mass balance over 2070–2100 with that over 1970–2000. We assume that changes in ice thickness represent net mass-balance changes, that changes in cumulative surface flux reflect surface mass balance and that cumulative sub-ice-shelf flux corresponds to basal mass balance. Subtracting the last two terms from the net change in thickness gives an estimate of dynamic losses, which can be equated with loss due to iceberg calving. Using this approach we see that under RCP8.5 with melt feedbacks incorporated net mass balance by the end of the century decreases in almost all Antarctic and Greenland catchments. Several East Antarctic drainage basins experience increasing precipitation and a weakly positive surface mass balance (Fig. 3a), but across the majority of West Antarctica and all of Greenland surface accumulation is reduced. Basal melting of floating ice accounts for a substantial proportion of Antarctic mass loss but is negligible for much of Greenland, except in northwest and northeast catchments. In Greenland, dynamic (calving) losses are greatest early in the century, before the reduction in surface mass balance begins to dominate from mid-century onwards (Fig. 1f, h).

Environmental consequences of ice-sheet melt

In Fig. 4 we show the environmental consequences by 2100 of adding meltwater fluxes from our two ice-sheet simulations to the adjacent ocean. Our climate model simulates globally important effects on surface air temperature (Fig. 4a), sea surface temperature (Fig. 4b), subsurface (415-m depth) ocean temperature (Fig. 4c) and sea surface height (Fig. 4h). The climate anomalies, calculated from the century-end 30-year mean (2090–2120) to smooth out short-term variability, are solely the consequence of the addition of ice-sheet melt from ice-sheet simulations under RCP8.5, compared to a climate simulation in which no melt is added but which is otherwise identical. Radiative forcing is held constant, so the patterns of thermal anomalies arise entirely from changes in ocean mixing and/or atmospheric circulation. Air temperature anomalies (Fig. 4a) are strongly differentiated between northern and southern high latitudes. In the north, warming occurs over the Greenland Sea (northeast of Greenland) in the region of Svalbard, and as far north as the North Pole (Extended Data Fig. 1a). In the Southern Hemisphere, widespread air surface cooling of more than 2 °C and local cooling of up to 4 °C is evident south of approximately 40° S (Extended Data Fig. 1b). Air temperature anomalies reflect the pattern of changes predicted in surface ocean temperatures (Fig. 4b), although the latter are of lower magnitude. Ocean temperature changes at 415-m depth (Fig. 4c)—relevant for Antarctic grounding lines—are negative through much of the Southern Ocean away from Antarctica, but widespread warming occurs in mid- to low latitudes and in areas where freshwater fluxes are applied close to the simulated ice sheets. Substantial subsurface warming (0.5–1.0 °C) is evident around much of the Antarctic continent, with maxima in the Ross Sea, along the coast of West Antarctica and around the western Antarctic Peninsula (Extended Data Fig. 1a, b).

Our simulations allow the influence of the meltwater feedback to be isolated, but do not incorporate the warming from radiative forcing associated with likely future increases in greenhouse gas emissions. To gauge whether the melt feedback mechanism that we investigate is

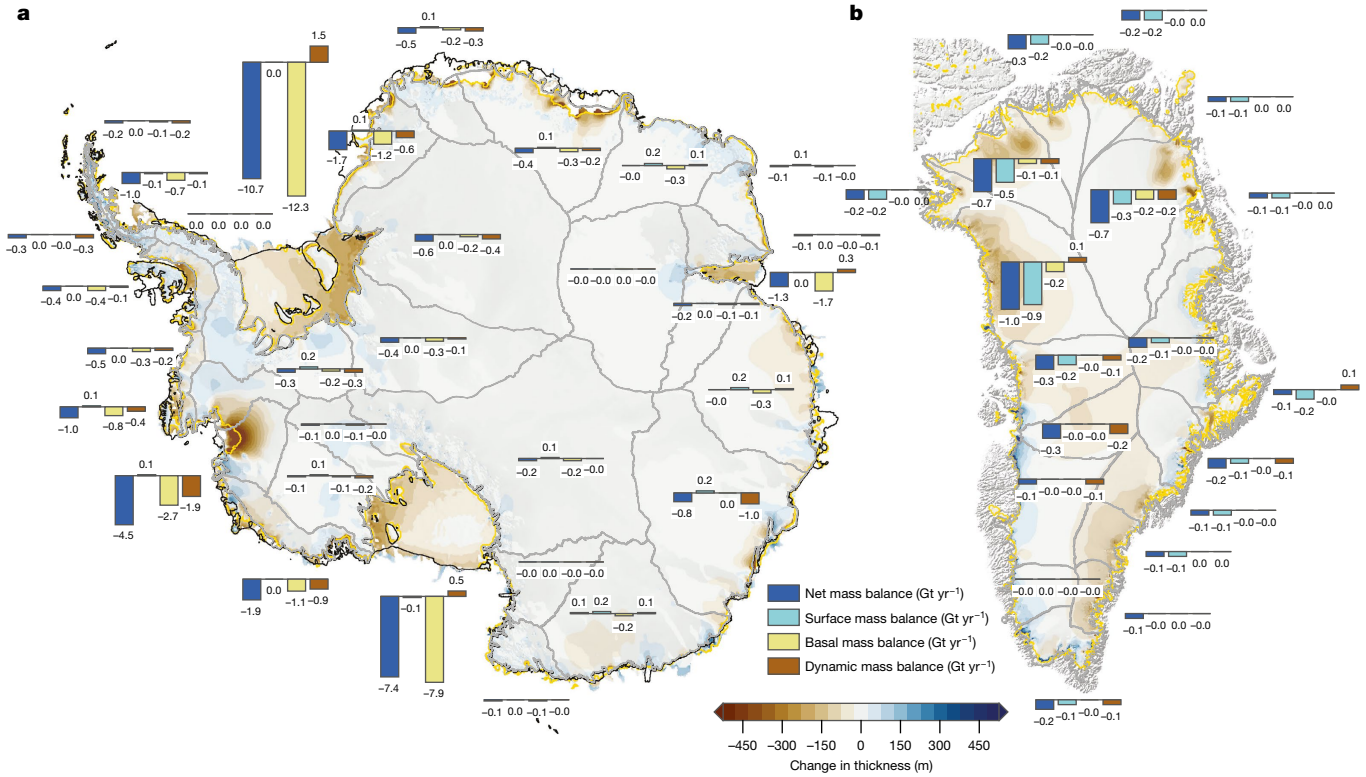

Fig. 3 | Causes of changes in ice-sheet thickness by 2100. a, **b**, Simulated patterns of changes in ice-sheet thickness by 2100, compared to 2000, in Antarctica (**a**) and Greenland (**b**) under RCP8.5 and incorporating ice–ocean–atmosphere feedbacks. Note the widespread ice-shelf thinning and retreat of Thwaites Glacier in Antarctica (**a**) and the peripheral thinning around much of the Greenland Ice Sheet (**b**). Bar charts attribute mass change to individual mass-balance components, for each ice-sheet catchment (see text). Mass loss values are calculated as the difference between the catchment-integrated annual total at 2100 and at 2000. Grey lines denote the outlines of the ice-sheet drainage basins (Methods). Thin black lines show the present-day grounding-line and calving-line positions (Methods). Gold lines show modelled grounded-ice margins at 2100.

globally, or only locally, important, we compare the magnitude of our predicted changes with anomalies from CMIP5 data in which emissions forcing is implemented but no meltwater fluxes are included (Extended Data Fig. 2). This comparison illustrates that even the modest combined ice-sheet discharge volume we predict (less than 0.2 Sv at 2100) is sufficient to modify CMIP5-predicted air and sea surface temperatures by as much as 10% in some areas. These anomalies, as well as our predicted reduction of approximately 0.3 °C in the increase in global-mean air temperature by 2100 (Extended Data Fig. 2), are very consistent with findings from other scenario-based simulations[30].

Perhaps more immediately impactful than gradual warming is the possibility of enhanced interannual temperature variability, which would result in more widespread or more frequent terrestrial and marine heat waves. Such events affect ecosystems directly[31,32] and may contribute to long-term changes in Arctic sea-ice thickness[33]. Our coarse-resolution climate model is unable to fully capture short-term weather events, but can still give an indication of whether the inclusion of ice-sheet meltwater fluxes in higher-resolution models would greatly affect predicted interannual variability (Methods). Compared to control simulations, the inclusion of ice-sheet melt leads to substantial changes in the amplitude of interannual variability (more than 50%) across the globe, resulting in considerable disruption to annual- to decadal-scale climate patterns (Fig. 4e–g).

To predict the spatial pattern of sea-level change during the twenty-first century, we use a global sea-level model that includes gravitational self-consistency, Earth rotation and deformation of a radially varying viscoelastic Earth (Fig. 4d, Extended Data Fig. 1c). Predicted sea-level changes are largest and most spatially variable near the ice sheets, in particular in Antarctica where changes in ice mass around the periphery of the ice sheet are also variable. Reduced gravitational attraction and uplift of the solid Earth leads to a shallowing of the oceans in regions of ice loss such as the Amundsen Sea embayment, and the reverse leads to sea-level rise in regions of localized ice gain such as near mountainous areas of the Antarctic Peninsula. Our sea-level model predicts that by 2100 the largest area of high sea-level rise from ice-sheet melt (more than 0.3 m) should occur in the central Pacific Ocean (Fig. 4d). Much of the mid- to low latitudes also experience sea levels around 0.3 m higher than in the year 2000. When thermosteric effects (calculated in our climate model) that arise from meltwater-induced oceanic changes are included, a more complex pattern of sea-level rise emerges (Fig. 4h, Extended Data Fig. 1d). In this instance, changes in the distribution of ocean heat (primarily at depth; Fig. 4b, c) lead to substantial changes in sea surface height in some areas, such as in the open ocean around Antarctica (Extended Data Fig. 1d). However, in most areas close to the ice sheet, rotational or gravitational effects dominate thermosteric changes.

Influence of ice-sheet melt on AMOC

In the North Atlantic, our simulated pattern of temperature anomalies most probably arises from a slowdown of the upper cell of the AMOC driven by meltwater from the Greenland Ice Sheet (Fig. 5a). Theoretical analysis and model studies indicate that the AMOC is a highly nonlinear system that is sensitive to changes in freshwater forcing[34]. Specifically, gradual increases in freshwater bring AMOC strength to a bifurcation point (saddle node) beyond which no positive stable state is possible and overturning reduces to near zero[34,35]. Recent research has identified a measureable slowdown since pre-industrial times[7,8] and simulations of future changes predict continued weakening, and potential collapse, under unmitigated emissions scenarios[36]. Although our Greenland-derived meltwater fluxes are too low (about 0.018 Sv under RCP8.5 with melt feedback) to trigger a collapse of the overturning circulation this century, we see a substantial reduction in strength by 2100. In our experiments a gradual slowing in the first half of the century steepens after 2050, leading to a reduction in AMOC strength

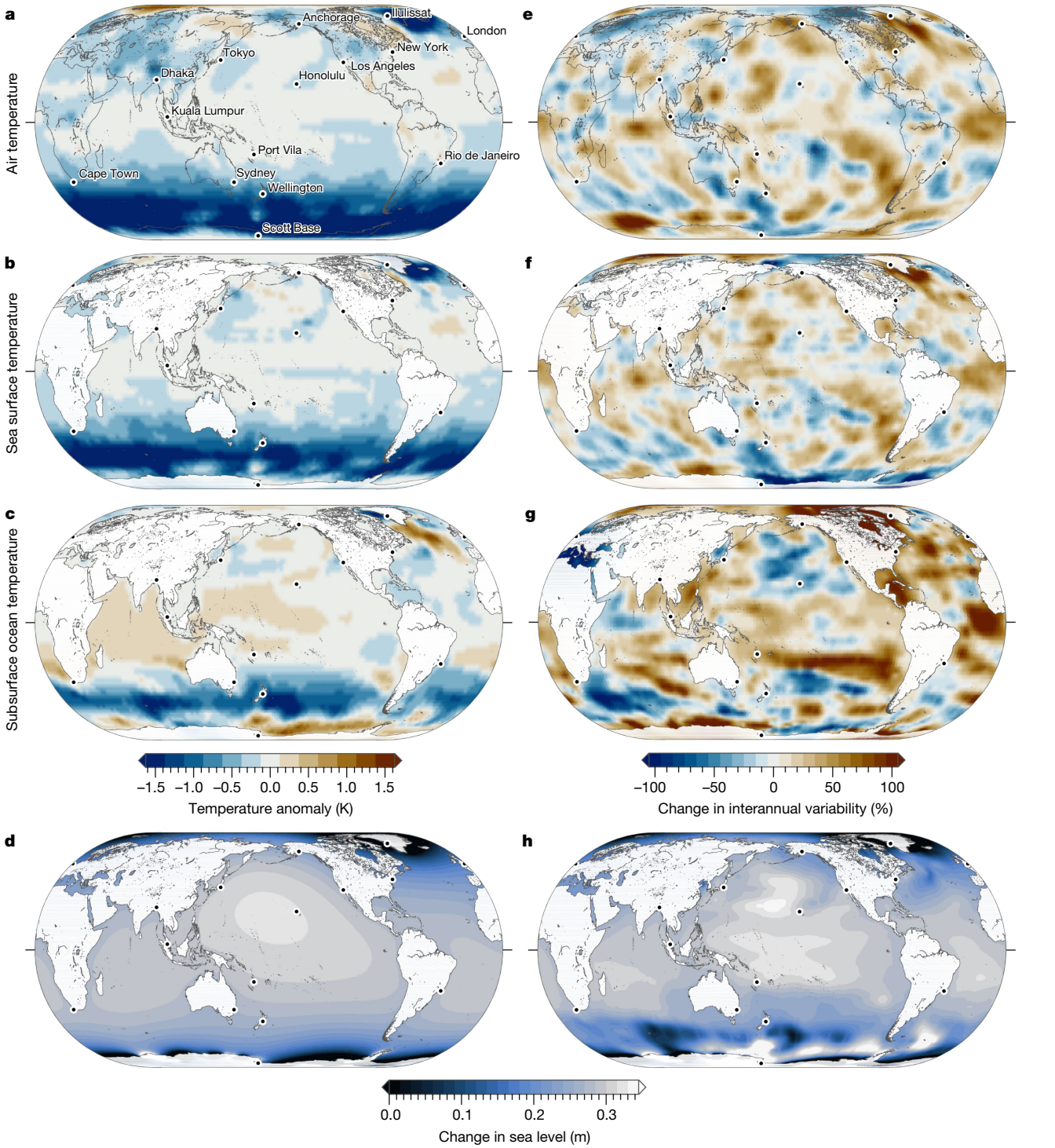

Fig. 4 | Environmental consequences of twenty-first-century ice-sheet meltwater flux. a–d, Modelled patterns at 2100 of changes in air temperature (**a**), sea surface temperature (**b**), subsurface (415-m depth) ocean temperature (**c**) and sea level (**d**), compared to 2000, that arise solely from mixing and circulation changes due to the input of ice-sheet melt simulated under RCP8.5 with ice–ocean–atmosphere feedbacks. Various cities are labelled for reference. Anomalies are 30-year means to avoid aliasing short-term variability. Note substantial air and sea surface cooling around Antarctica (**a**, **b**) and the contrasting warming of the subsurface ocean close to the coast (**c**). Subsurface warming is also evident in parts of the Arctic. Extended Data Fig. 1a, b shows polar perspectives. **e–g**, Magnitude of changes in interannual temperature variability by 2100, compared to 2000, due to the addition of meltwater. **h**, Sum of modelled sea-level rise (**d**) and predicted changes in sea surface height by 2100 arising from thermosteric effects of meltwater input under RCP8.5 with ice–ocean–atmosphere feedbacks.

of 3–4 Sv (approximately 15%) over 50 years. This occurs purely as a consequence of the imposed meltwater fluxes and so would presumably add to any weakening from future climate forcing. The lower (anticlockwise) cell of the AMOC is weaker and responds more slowly, with changes in this instance being forced primarily by Antarctic meltwater (Fig. 5b). Because current climate models are thought to overestimate the stability of the AMOC[37], it is possible that future ice-sheet meltwater fluxes may have an even more important role than we predict here. Simulations extended to 500 years but without the second iteration of meltwater feedback show an abrupt recovery of the AMOC after approximately 300 years (Fig. 5a, b), in agreement with other studies[38].

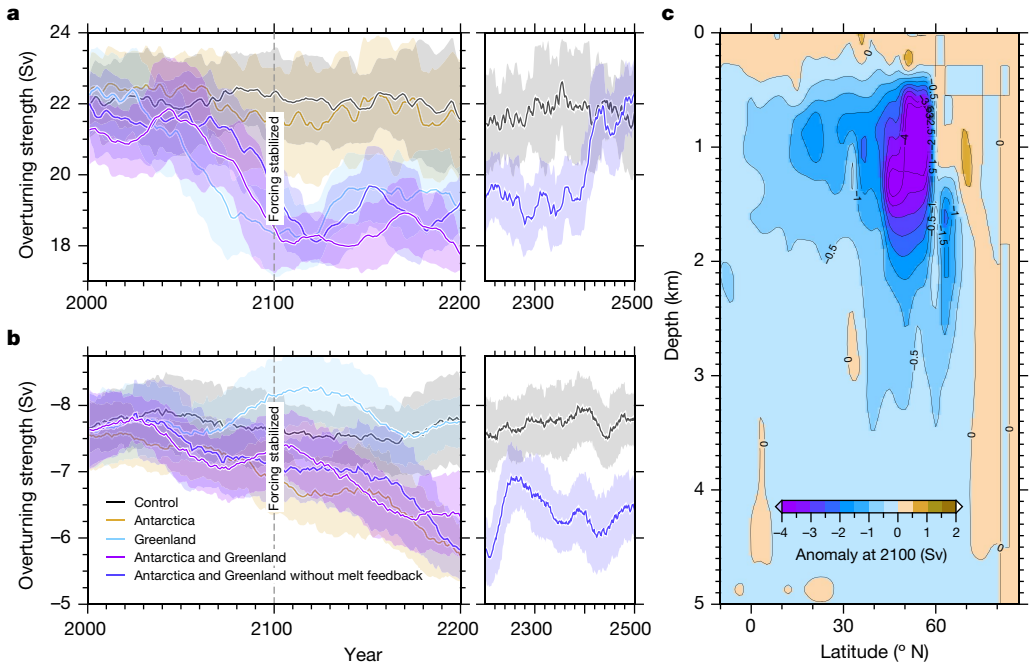

Fig. 5 | Effect of ice-sheet melt on the AMOC. a, **b**, Changes in the overturning strength of clockwise (**a**) and anticlockwise (**b**) components of the AMOC that arise in the second climate model iteration, which incorporates ice–ocean–atmosphere feedbacks in an ice-sheet simulation under RCP8.5. Overturning strength is defined as the maximum (clockwise) and minimum (anticlockwise) of the meridional overturning stream function in the Atlantic Ocean basin in each year. Effects vary depending on whether added meltwater originates from only the Greenland Ice Sheet (light blue), only the Antarctic Ice Sheet (gold) or from both ice sheets (purple). Black lines illustrate a control simulation in which no meltwater is added. Dark blue lines (running to 2500) show results from the first iteration of the ice-sheet and climate simulations, in which ice–ocean–atmosphere feedbacks on the ice sheet are not included. All curves are 30-year running means; shaded envelopes represent the evolving 30-year standard deviation of annual data. The vertical lines at 2100 indicate the time after which environmental forcings are held constant in our simulations. **c**, Anomalies in the overturning strength at 2100 compared to a control run with no ice-sheet meltwater added. Anomalies are 30-year means to avoid aliasing short-term variability. The decrease of roughly 4 Sv in AMOC strength at depths of 0.5–1.5 km takes place over approximately 50 years (see **a**).

Discussion

Our results arise from an experimental set-up that (1) is underpinned by time-varying multi-parameter present-day measurements (Fig 1), (2) predicts twenty-first-century ice-sheet mass loss in areas where recent thinning has been greatest (Fig. 3) and (3) allows more extreme Antarctic scenarios such as warm interglacial conditions of the early to mid-Pliocene to be reproduced (Extended Data Fig. 3). In addition, by using a parameterization that includes sub-grid melting at glacial grounding lines (Methods), our model produces a sea-level contribution from the Antarctic Ice Sheet of 0.14 m by 2100, which compares favourably with the mode (0.15 m; 90% probability interval, 0.09–0.39 m) for the same scenario derived from a reanalysis of previous simulations[20] in which marine ice-cliff instability is excluded[39]. Further, the timing of a positive Antarctic sea-level contribution is almost identical in our study and the reanalysis[39], with both identifying the emergence of a clear signal during the middle of the century.

However, in our simulation of the Greenland Ice Sheet we need to impose two time-varying modifications to obtain a good fit to observational constraints. From 2000 to 2025 we gradually reduce the snowpack refreezing coefficient in our model, such that the surface mass-balance trajectory is well captured. This modification is based on previous work that identified that a reduction in refreezing has already taken place in outlying Greenlandic icefields[40] and the main ice sheet[41], and is expected to reduce further in the future as the area of bare ice increases[42]. Even with the surface mass balance well represented, fitting to overall net mass-balance constraints requires further modification of model parameters. Observations suggest that recent warm-water incursions in certain fjords or increased meltwater at the ice-sheet bed may be responsible for increased dynamic thinning[43,44]. Although we have no robust way to constrain short-term spatially variable ocean warming anomalies, by applying a tapered reduction of the basal traction coefficient (reaching a maximum of −40% relative to its initial value) during the period 2000–2015 we are able to increase dynamic thinning and so match the observed mass loss profile (Methods section 'Experimental methods', Extended Data Fig. 5d). This simple approach preferentially accelerates flow in outlet glaciers, where basal sliding is highest, much as would occur if warmer waters led to thinning of the marine terminus. Different parameterizations lead to different initial trajectories, but all are followed by stabilization. This leads us to concur with previous studies[43,44] that future mass loss from Greenland (especially in the latter half of the century in our RCP8.5 simulation) will be dictated primarily by declining net surface accumulation (Fig. 3b), because retreat of marine-terminating glaciers isolates such margins from ocean-driven melt and is therefore a self-limiting process.

In Antarctica, forecast mass losses arise from increasing ice-shelf basal melt and increased iceberg calving of West Antarctic glaciers. We predict the greatest mass loss in the Amundsen Sea sector, primarily associated with thinning and recession of Thwaites Glacier, as predicted in other studies[45]. Our stabilization scenarios illustrate that, even with ocean temperatures held constant from 2020 and without including meltwater feedback, the loss of a substantial portion of the West Antarctic Ice Sheet may already be committed (Extended Data Fig. 4). However, the rate of future greenhouse gas emissions will dictate the magnitude and timing of this committed loss. Our simulations show areas of positive surface mass balance across some drainage basins of the East Antarctic Ice Sheet, in line with modern observations[1,46]. In contrast to previous studies[18,20], we do not see a collapse of the Filchner–Ronne or Ross ice shelves by 2100, even under RCP8.5. Our observation-constrained melt model instead predicts widespread and substantial thinning, together with increased calving, but very little change in overall extent. However, we do simulate a loss of the Larsen C ice shelf and many of the ice shelves that fringe Dronning

Maud Land. Our model does not include the mechanics of ice-shelf hydrofracture or cliff failure[20], which might hasten retreat. However, it is our contention that such processes are unlikely to be important during this century; this is based on three lines of evidence. First, by incorporating ice–ocean–atmosphere feedbacks, our simulations predict substantial atmospheric cooling over mid- to high southern latitudes (Extended Data Fig. 1b), which will offset approximately 0.5–3.5 °C of the atmospheric warming predicted by CMIP5 models (Extended Data Fig. 2c, d) and thus reduce melt. Second, although we do not have data from warmer-than-present conditions, contemporary observations show that surface melt has been a normal component of Antarctic ice shelves in the recent past, without it having led to shelf breakup[47,48]. Third, simulations of future surface melting across Antarctic ice shelves using regional climate models such as RACMO2.1 (ref. [49]) and CMIP5 general circulation models[50] predict far lower melt quantities than the simulations of ref. [20]. If such high melt is necessary to induce continent-wide hydrofracture, then these other models would imply that more extreme atmospheric warming than predicted for 2100 may be necessary to trigger widespread ice-shelf collapse.

Regardless of the precise magnitude of future ice-sheet discharge, the redistribution of ocean heat and effects of the rotation, gravitation and deformation of Earth mean that sea-level rise will most substantially affect mid- to low-latitude island nations in both hemispheres. Ice–ocean–atmosphere feedbacks simulated in our models suggest that subsurface ocean warming will increase grounding-line retreat around Antarctica and may enhance basal melting of sea ice in the Arctic[33]. By mid-century in our simulations, meltwater from the Greenland Ice Sheet noticeably disrupts the AMOC, which could exacerbate the recently observed slowing trend[7]. Globally, the inclusion of ice-sheet meltwater fluxes in climate simulations appears to result in a complex pattern of atmospheric and oceanic changes that include heightened interannual variability in some areas, which could result in more frequent extreme weather events.

Online content

Any methods, additional references, Nature Research reporting summaries, source data, statements of data availability and associated accession codes are available at https://doi.org/10.1038/s41586-019-0889-9.

Received: 6 July 2018; Accepted: 21 December 2018;
Published online 6 February 2019.

1. The IMBIE team. Mass balance of the Antarctic Ice Sheet from 1992 to 2017. *Nature* **558**, 219–222 (2018).
2. Forsberg, R., Sørensen, L. & Simonsen, S. Greenland and Antarctic Ice Sheet mass changes and effects on global sea level. *Surv. Geophys.* **38**, 89–104 (2017).
3. Chen, X. et al. The increasing rate of global mean sea-level rise during 1993–2014. *Nat. Clim. Chang.* **7**, 492–495 (2017).
4. Huss, M. & Hock, R. A new model for global glacier change and sea-level rise. *Front. Earth Sci.* **3**, 54 (2015).
5. Bamber, J. L., Westaway, R. M., Marzeion, B. & Wouters, B. The land ice contribution to sea level during the satellite era. *Environ. Res. Lett.* **13**, 063008 (2018).
6. Dieng, H. B., Cazenave, A., Meyssignac, B. & Ablain, M. New estimate of the current rate of sea level rise from a sea level budget approach. *Geophys. Res. Lett.* **44**, 3744–3751 (2017).
7. Caesar, L., Rahmstorf, S., Robinson, A., Feulner, G. & Saba, V. Observed fingerprint of a weakening Atlantic Ocean overturning circulation. *Nature* **556**, 191–196 (2018).
8. Thornalley, D. J. R. et al. Anomalously weak Labrador Sea convection and Atlantic overturning during the past 150 years. *Nature* **556**, 227–230 (2018).
9. Raftery, A. E., Zimmer, A., Frierson, D. M. W., Startz, R. & Liu, P. Less than 2 °C warming by 2100 unlikely. *Nat. Clim. Chang.* **7**, 637–641 (2017).
10. Lenton, T. M. et al. Tipping elements in the Earth's climate system. *Proc. Natl Acad. Sci. USA* **105**, 1786–1793 (2008).
11. Rignot, E., Mouginot, J., Morlighem, M., Seroussi, H. & Scheuchl, B. Widespread, rapid grounding line retreat of Pine Island, Thwaites, Smith, and Kohler glaciers, West Antarctica, from 1992 to 2011. *Geophys. Res. Lett.* **41**, 3502–3509 (2014).
12. Joughin, I., Smith, B. E. & Medley, B. Marine ice sheet collapse potentially under way for the Thwaites Glacier basin, West Antarctica. *Science* **344**, 735–738 (2014).
13. Vitousek, S. et al. Doubling of coastal flooding frequency within decades due to sea-level rise. *Sci. Rep.* **7**, 1399 (2017).
14. King, A. D. & Harrington, L. J. The inequality of climate change from 1.5 to 2 °C of global warming. *Geophys. Res. Lett.* **45**, 5030–5033 (2018).
15. Kopp, R. E. et al. Evolving understanding of Antarctic ice-sheet physics and ambiguity in probabilistic sea-level projections. *Earths Futur.* **5**, 1217–1233 (2017).
16. Jackson, L. P., Grinsted, A. & Jevrejeva, S. 21st century sea-level rise in line with the Paris Accord. *Earths Futur.* **6**, 213–229 (2018).
17. Ritz, C. et al. Potential sea-level rise from Antarctic ice-sheet instability constrained by observations. *Nature* **528**, 115–118 (2015).
18. Golledge, N. et al. The multi-millennial Antarctic commitment to future sea-level rise. *Nature* **526**, 421–425 (2015).
19. Vizcaino, M. et al. Coupled simulations of Greenland Ice Sheet and climate change up to A.D. 2300. *Geophys. Res. Lett.* **42**, 3927–3935 (2015).
20. DeConto, R. & Pollard, D. Contribution of Antarctica to past and future sea-level rise. *Nature* **531**, 591–597 (2016).
21. Weaver, A. J. et al. Stability of the Atlantic meridional overturning circulation: a model intercomparison. *Geophys. Res. Lett.* **39**, L20709 (2012).
22. Collins, M. et al. in *Climate Change 2013: The Physical Science Basis. Contribution of Working Group I to the Fifth Assessment Report of the Intergovernmental Panel on Climate Change* (eds Stocker, T. et al.) 1029–1136 (Cambridge Univ. Press, Cambridge, 2013).
23. Bintanja, R., van Oldenborgh, G. J. & Katsman, C. A. The effect of increased fresh water from Antarctic ice shelves on future trends in Antarctic sea ice. *Ann. Glaciol.* **56**, 120–126 (2015).
24. Bueler, E. & Brown, J. Shallow shelf approximation as a "sliding law" in a thermomechanically coupled ice sheet model. *J. Geophys. Res.* **114**, F03008 (2009).
25. Bernales, J., Rogozhina, I. & Thomas, M. Melting and freezing under Antarctic ice shelves from a combination of ice-sheet modelling and observations. *J. Glaciol.* **63**, 731–744 (2017).
26. Golledge, N. et al. Antarctic contribution to meltwater pulse 1A from reduced Southern Ocean overturning. *Nat. Commun.* **5**, 5107 (2014).
27. Bakker, P., Clark, P. U., Golledge, N. R., Schmittner, A. & Weber, M. E. Centennial-scale Holocene climate variations amplified by Antarctic Ice Sheet discharge. *Nature* **541**, 72–76 (2017).
28. Menviel, L., Timmermann, A., Timm, O. E. & Mouchet, A. Climate and biogeochemical response to a rapid melting of the West Antarctic Ice Sheet during interglacials and implications for future climate. *Paleoceanography* **25**, PA4231 (2010).
29. Weber, M. et al. Millennial-scale variability in Antarctic ice-sheet discharge during the last deglaciation. *Nature* **510**, 134–138 (2014).
30. Bronselaer, B. et al. Change in future climate due to Antarctic meltwater. *Nature* **564**, 53–58 (2018).
31. Frölicher, T. L., Fischer, E. M. & Gruber, N. Marine heatwaves under global warming. *Nature* **560**, 360–364 (2018).
32. Ruthrof, K. X. et al. Subcontinental heat wave triggers terrestrial and marine, multi-taxa responses. *Sci. Rep.* **8**, 13094 (2018).
33. Hutchings, J. K. & Perovich, D. K. Preconditioning of the 2007 sea-ice melt in the eastern Beaufort Sea, Arctic Ocean. *Ann. Glaciol.* **56**, 94–98 (2015).
34. Rahmstorf, S. Bifurcations of the Atlantic thermohaline circulation in response to changes in the hydrological cycle. *Nature* **378**, 145–149 (1995).
35. Stommel, H. Thermohaline convection with two stable regimes of flow. *Tellus* **13**, 224–230 (1961).
36. Bakker, P. et al. Fate of the Atlantic Meridional Overturning Circulation: strong decline under continued warming and Greenland melting. *Geophys. Res. Lett.* **43**, 12252–12260 (2016).
37. Liu, W., Xie, S.-P., Liu, Z. & Zhu, J. Overlooked possibility of a collapsed Atlantic Meridional Overturning Circulation in warming climate. *Sci. Adv.* **3**, e1601666 (2017).
38. Rind, D. et al. Multi-century instability of the Atlantic Meridional Circulation in rapid warming simulations with GISS ModelE2. *J. Geophys. Res.* **123**, 6331–6355 (2018).
39. Edwards, T. L. et al. Revisiting Antarctic ice loss due to marine ice-cliff instability. *Nature* **566**, https://doi.org/10.1038/s41586-019-0901-4 (2019).
40. Noël, B. et al. A tipping point in refreezing accelerates mass loss of Greenland's glaciers and ice caps. *Nat. Commun.* **8**, 14730 (2017).
41. Machguth, H. et al. Greenland meltwater storage in firn limited by near-surface ice formation. *Nat. Clim. Chang.* **6**, 390–393 (2016).
42. Fettweis, X. et al. Estimating the Greenland ice sheet surface mass balance contribution to future sea level rise using the regional atmospheric climate model MAR. *Cryosphere* **7**, 469–489 (2013).
43. Shannon, S. R. et al. Enhanced basal lubrication and the contribution of the Greenland ice sheet to future sea-level rise. *Proc. Natl Acad. Sci. USA* **110**, 14156–14161 (2013).
44. Fürst, J. J., Goelzer, H. & Huybrechts, P. Ice-dynamic projections of the Greenland ice sheet in response to atmospheric and oceanic warming. *Cryosphere* **9**, 1039–1062 (2015).
45. Seroussi, H. et al. Continued retreat of Thwaites Glacier, West Antarctica, controlled by bed topography and ocean circulation. *Geophys. Res. Lett.* **44**, 6191–6199 (2017).
46. Medley, B. et al. Temperature and snowfall in western Queen Maud Land increasing faster than climate model projections. *Geophys. Res. Lett.* **45**, 1472–1480 (2018).
47. Phillips, H. A. Surface meltstreams on the Amery ice shelf, East Antarctica. *Ann. Glaciol.* **27**, 177–181 (1998).

48. Bevan, S. L. et al. Centuries of intense surface melt on Larsen C ice shelf. *Cryosphere* **11**, 2743–2753 (2017).
49. Trusel, L. D. et al. Divergent trajectories of Antarctic surface melt under two twenty-first-century climate scenarios. *Nat. Geosci.* **8**, 927–932 (2015).
50. Bell, R. E., Banwell, A., Trusel, L. & Kingslake, J. Antarctic surface hydrology and impacts on ice sheet mass balance. *Nat. Clim. Chang.* **8**, 1044–1052 (2018).

Acknowledgements We acknowledge K. Buckley (Victoria University high-performance compute cluster), the Parallel Ice Sheet Model groups at University of Alaska, Fairbanks, the Potsdam Institute for Climate Impact Research and the CMIP community for making their data openly available. PISM is supported by NASA grants NNX13AM16G and NNX13AK27G. This work was funded by contract VUW1501 to N.R.G. from the Royal Society Te Aparangi, with support from the Antarctic Research Centre, Victoria University of Wellington, and GNS Science through the Ministry for Business, Innovation and Employment contract CO5X1001. N.G. was supported by the Natural Sciences and Engineering Research Council of Canada and the Canada Research Chairs programme. J.B. was supported by the MAGIC-DML project through DFG SPP 1158 (RO 4262/1-6). L.D.T. acknowledges support from the NSF Antarctic Glaciology Program (award 1643733).

Reviewer information *Nature* thanks F. Pattyn, H. Seroussi and the other anonymous reviewer(s) for their contribution to the peer review of this work.

Author contributions N.R.G. devised and carried out the ice-sheet modelling experiments, E.D.K. undertook climate model simulations and N.G. performed the sea-level calculations. K.A.N., J.B. and L.D.T. provided Antarctic basal and surface melt simulations from regional models. All authors contributed to the development of ideas and writing of the manuscript.

Competing interests The authors declare no competing interests.

Additional information
Extended data is available for this paper at https://doi.org/10.1038/s41586-019-0889-9.
Reprints and permissions information is available at http://www.nature.com/reprints.
Correspondence and requests for materials should be addressed to N.R.G.
Publisher's note: Springer Nature remains neutral with regard to jurisdictional claims in published maps and institutional affiliations.

METHODS

The ice-sheet model. We use the Parallel Ice Sheet Model[24,51,52] (PISM) version 0.7.3. PISM is a hybrid ice-sheet–ice-shelf model that combines shallow approximations of the flow equations that compute gravitational flow and flow by horizontal stretching. The combined stress balance allows for a consistent treatment of ice-sheet flow, from non-sliding grounded ice to rapidly sliding grounded ice (ice streams) and floating ice shelves. In common with most continental-scale ice-sheet models, PISM incorporates enhancement factors for each component of the stress regime, allowing creep and sliding velocities to be adjusted using simple coefficients. These are model constants and do not evolve. These enhancement factors enable simulations to be optimized such that modelled behaviour matches observed behaviour. The junction between grounded and floating ice is refined by a sub-grid-scale parameterization[53] that smooths the basal shear stress field and the basal melt. In previous simulations[18,54] we ran duplicate experiments with and without this interpolation of basal melting. Our experimentation revealed that the use of sub-grid melting increases the ability of glacier grounding lines to retreat, leading to faster ice loss. Although the numerical veracity of this approach has been questioned[55], we have previously found little evidence for a grid-size dependence in using this scheme[18] and find instead that it enables simulated mass loss under warmer-than-present palaeoclimate scenarios that is more closely in agreement with proxy reconstructions than when sub-grid melting is omitted[54]. In support of this approach are recent observations confirming that oceanic water intrudes into the grounding zone of marine-terminating Antarctic glaciers in some areas[56], carrying with it heat available for melting of ice. We optimize our model with this scheme and use it in all experiments, but acknowledge that this is an area in which our simulations may introduce uncertainties. To quantify these uncertainties, we ran our control and RCP8.5 simulations for both ice sheets with and without the sub-grid melt scheme (Extended Data Fig. 5a, b). These results suggest that while the sub-grid scheme has little influence in Greenland, our Antarctic runs produce mass-loss forecasts approximately 40% lower when sub-grid melting is not used. However, our control experiment in these simulations exhibits more substantial deviation from present-day ice volume, suggesting that other parameters may need adjustment to accurately capture Antarctic Ice Sheet evolution without use of the sub-grid melt scheme. We run our experiments at grid resolutions of 2.5 km (Greenland) and 5 km (Antarctica). By adopting such high resolutions, together with the sub-grid grounding-line scheme described above, our model is able to accurately track grounding-line migration[53]. We find little evidence of grid dependence in the 5–20-km range, both in previous simulations[18] and in the experiments presented here (Extended Data Fig. 5c).

Mass balance at the ice surface is computed by a positive degree-day algorithm that uses degree-day factors of 2 mm $°C^{-1}$ day^{-1} and 4 mm $°C^{-1}$ day^{-1} for the melting of snow and ice, respectively. These very low values are used in conjunction with a positive threshold temperature of 270 K, rather than the usual 273 K—a combination that has been shown to better reproduce the spatial distribution of surface melting (in Greenland) than achieved with higher melt factors and a higher threshold temperature[57]. We use a standard deviation of daily temperature variability of 2.5 K, and a refreezing coefficient of 0.6 to account for retention of surface melt within the snow or firn, but we vary this coefficient in our Greenland optimization to match our predicted surface melt trajectory to empirical constraints. This approach is underpinned by the recognition of recent and forecast changes in refreezing in Greenland[40–42]. Basal mass balance is calculated using a thermodynamic model that reads temperature and salinity values and calculates a melt rate[58]. In our implementation of PISM it is only possible to use a single ocean temperature field; we therefore sought to improve the way in which present-day melt fields can be more accurately captured. Specifically, we make a substantial advance over our previous simulations[18] in terms of accurately capturing present-day Antarctic ice shelf basal melt rates by using an empirically tuned melt simulation[25] to calculate a melt factor. We run an iteration in which we input present-day sea surface temperatures from CMIP5 outputs, and then incrementally adjust our melt factor at each grid point to reduce the mismatch between observed melt values (our 'target') and values calculated using the melt scheme (Extended Data Fig. 5c, d). Our dimensionless coefficient is otherwise unconstrained and may be a source of error when applied to future changes in temperature. However, this simple approach yields predicted melt rates under present-day conditions that match observed values far more closely than melt schemes that are not optimized[18,20]. The consequence of this method is that we correctly simulate the 'cold' cavities of the Ross and Ronne–Filchner ice shelves, while also capturing the very high melt rates witnessed in the Amundsen Sea proximal to Thwaites and Pine Island glaciers. We acknowledge, however, that the strength of this approach relies on the relationship between temperature, our melt factor and the derived melt rate remaining unchanged through time. Because the relationship between water temperature and melt rate is highly variable around Antarctica[59], we do not expect to fully capture all possible scenarios, but instead aim for an improvement over previous simplifications[18,20]. Future ocean circulation changes that are not captured in CMIP5-modelled temperature anomalies may also lead to greater temperature changes in some areas that we are unable to account for with our simple scheme, which may affect our results. An additional simplification in our approach is that, in the absence of a dynamically coupled high-resolution ice-shelf cavity-resolving ocean model, we are restricted to interpolating our ocean temperature anomalies landward, which will not accurately capture topographic funnelling of ocean currents that may focus melt in certain areas[60]. Iceberg calving is calculated in our model using two schemes. In the first, horizontal strain rates are used to derive calving rates, leading to faster calving in areas of fast flow[61]. The second scheme applies a simple but heuristic minimum-thickness criterion to ensure that thin floating ice is removed. In our spin-up experiment we used a minimum thickness of 200 m, which allowed the major ice shelves to be well represented. However, to ensure that thinner ice shelves were not automatically lost during our RCP-forced experiments, we reduced this thickness limit to 50 m. To reproduce the empirical constraints on calving fluxes as closely as possible (Fig. 1d, h), we incrementally adjusted the strain rate exponent ensuring that observed calving-front locations were also accurately maintained under present-day conditions.

Present-day conditions. For input data to our ice-sheet model we use the most up-to-date environmental datasets available. Our ice thickness and bed topography are from BEDMAP2 for Antarctica[62] and from BedMachine v.3 for Greenland[63]. Climatologies come from RACMO2.3[64] (Antarctica) and RACMO2/GR[65] (Greenland). Ocean temperatures are derived for both model domains from CMIP5 simulations of present-day climate, which in Antarctica are combined with the melt factor described above to generate accurate melt rates. Oceanic fields are less well constrained for our Greenland domain because an accurate present-day basal melt map is not available for our inversion. Consequently, we use a uniform melt factor, adjusted so that present-day grounding-line positions are well captured. Because basal melting has a less important role in Greenland than in Antarctica, we are satisfied that this simplification is justified. Geothermal heat flux maps are taken from ref. [66] for Antarctica and ref. [67] for Greenland.

Future climate trajectories. For our simulations of ice-sheet evolution throughout the twenty-first century, we use the same CMIP5 multi-model-mean climate and ocean fields as used previously[18], but with the important difference that we use spatially varying fields for air temperature, precipitation and sea surface temperature rather than domain-averaged time series. Furthermore, we use monthly resolution surface climate fields for the entire period of our simulations (1860–2100) and use annual fields for our ocean temperatures on the basis that ice-sheet response is affected primarily by interannual variability, rather than seasonal fluctuations that may not be well captured in the CMIP5 data. CMIP5 models are particularly prone to biases in the Antarctic region[68–70], so care must be taken when selecting models to use as forcing for the ice sheet. We chose the CMIP5 multi-model mean to force our simulations because it has been shown to best agree with present-day atmospheric reanalyses over the Southern Ocean and Antarctica[71]. Our focus in these experiments is quantifying ice-sheet evolution through the current century. However, we are also interested in long-term commitments; to that end we run a series of experiments in which we stabilize climate and ocean forcings at 2020, 2050 or 2100, and run the simulations under constant forcings to 2500. We consider only two RCPs, RCP4.5 and RCP8.5, because these scenarios effectively bracket the range of global-mean temperature increase that current policies and pledges commit us to (https://climateactiontracker.org/).

Climate and ocean model. Climate simulations were performed with the model LOVECLIM v1.3[72]. LOVECLIM (LOch–Vecode–Ecbilt–CLio–agIsm-Model) is an intermediate-complexity Earth system model with coupled atmosphere, ocean/sea ice and dynamic vegetation. The atmospheric model ECBilt is a three-dimensional, spectral T21 model, with three vertical levels and 5.6° horizontal resolution. The ocean component is CLIO—a free-surface primitive equation model with a 3° × 3° horizontal grid resolution and 20 vertical levels, which uses the Gent–McWilliams eddy advection parameterization[73]. CLIO includes a dynamic–thermodynamic sea ice model. The dynamic vegetation model is VECODE. The ocean carbon cycle component LOCH was turned off in these simulations because we are primarily interested in the dynamic physical response of the ocean and atmosphere rather than the biogeochemical aspects.

Although this intermediate-complexity model is simple in its representation of the ocean and atmosphere, it is well established and is used extensively[26,28,29,72,74–76]. In chapter 8 of the Fourth Assessment Report of the IPCC[77], comparison of intermediate-complexity models (including LOVECLIM) with more sophisticated general circulation models (GCMs) revealed that both exhibited similar scatter in their results, and both tended to produce results that, "...agree with observational estimates" (chapter 8.8.3). It was also found that in experiments involving a doubling of atmospheric CO_2 the results from intermediate-complexity models fell within the range of results from GCMs, implying that their ability to capture climate anomalies was at least on par with the GCMs investigated in that assessment. Despite this, we interpret our climate fields with caution and focus primarily on the quantification of within-model anomalies (that is, the difference between

a perturbed and a control simulation, using the same model and taking 30-year-mean climate states to avoid short-term climate variability). This approach should reduce any potential biases inherent in the climate model.

The model was spun up with pre-industrial conditions for 1,000 years and then run from 1950 to 2000, forced with historical CO_2 atmospheric concentrations. The control simulation was continued from this initial state and run for 200 years, holding CO_2 constant at the 2000 level (370 p.p.m.). Simulations that used freshwater flux perturbations were started from the same initial state and forced with the same constant CO_2 level, but meltwater was added on a yearly basis in the form of a change in the local salinity of the ocean, at a rate prescribed by the output from the ice-sheet simulations until 2100. The freshwater flux was then held constant for an additional 100 years at the level reached in the last year of ice-sheet output. Freshwater fluxes were added separately for the Greenland and West Antarctic ice sheets, and distributed spatially using a mask in the North Atlantic (Greenland Ice Sheet) and from the Ross to the Weddell seas of Antarctica (West Antarctic Ice Sheet). Our Greenland mask applies meltwater to ocean cells in a box spanning 26–43° W, 62–90° N. In Antarctica, the box spans 160–360° E, 64–79° S. Mask extents were defined broadly to capture the effects of (unmodelled) iceberg melting. Ice-sheet extent and elevation were held fixed at present-day boundaries in all simulations. We ran two additional simulations including meltwater fluxes only from the Greenland Ice Sheet and only from the West Antarctic Ice Sheet to determine the influence of each individually (Fig. 5, Extended Data Fig. 6). Spatial outputs are shown as 30-year-mean climatologies from 2090 to 2120.

Sea-level model. Sea-level projections are calculated with a previously described global sea-level model[78]. The model includes gravitational self-consistency, viscoelastic deformation of an elastically compressible solid Earth, changes in rotation of the Earth, migrating shorelines and inundation of water into areas free of (grounded) marine-based ice. Initial topography in the simulations is given by ETOPO1 globally and replaced by the initial bedrock elevation predicted beneath the Greenland and Antarctic ice sheets within each ice-sheet model domain. Changes in ice thickness predicted with the Greenland and Antarctic ice-sheet models are combined into a global field, smoothed using a Gaussian smoother and interpolated onto a global, Gauss–Legendre grid with 512 points in latitude and 1,024 points in longitude. The interpolated grids are scaled to preserve total ice volume and passed to the sea-level model to compute sea-level changes every 5 years with a resolution of up to spherical harmonic degree and order 512. Rheological structure of the solid Earth in the model varies radially. Elastic and density structure is taken from the Preliminary Reference Earth Model (PREM)[79] and viscosity structure is defined by a 120- km-thick lithosphere and 100-km-thick upper and lower mantle with viscosities of 5×10^{20} Pa s and 5×10^{21} Pa s, respectively. This viscosity model falls within a class of one-dimensional viscosity profiles that are consistent with a wide range of global datasets related to ice-age glacial isostatic adjustment[80–82]. In the 100-year calculations presented here, however, the results are relatively insensitive to the choice of viscosity profile within the aforementioned class. Finally, sea-level changes computed at 5-year intervals are normalized and scaled by the global-average sea-level values computed at the native resolution of the ice-sheet model.

Experimental methods. For both of our model domains, we start our experiment with a long spin-up procedure in which we take present-day input fields and allow our ice sheets to evolve under palaeoclimate temperature forcings that represent the last glacial cycle. The purpose of these simulations is to allow the thermal structure of the ice sheets to evolve over a sufficiently long period that even deep layers of the ice sheets are influenced by changing atmospheric conditions. We adopt a hierarchical grid-refinement approach during this spin-up that includes a 'nudging' technique[83], so that when we increase the resolution of the model domains incrementally we also reset bed topography and ice thicknesses to present-day values. Our procedure for both model domains involves the following steps: (1) an initial smoothing run at 20-km resolution (5 years for Greenland, 20 years for Antarctica); (2) a fixed geometry and climate at 20-km resolution for 130,000 years; (3) an evolving geometry and transient forcing of climate at 20-km resolution from 130,000 years ago to 5,000 year ago; (4) a topography update to present-day, with grid refinement to 10-km resolution and palaeoclimate forcing from 4,000 years ago to 1,000 years ago; (5) a topography and ice-thickness update to present-day, with grid refinement to 5-km resolution and palaeoclimate forcing from 1,000 years ago to present-day; and (6) a topography and ice-thickness update to present-day, with grid refinement to 2.5-km resolution for Greenland and 5-km resolution for Antarctica, run for 500 years under present-day climate.

The advantage of this approach is that it allows the thermal fields evolved during the long spin-up to be remapped back onto the present-day ice thickness fields, thereby minimizing the mismatch between modelled and observed geometries at the end of the simulation and avoiding the unintended smoothing of bedrock topography that occurs during the low-resolution spin-up. By adopting multiple iterations of grid refinement and ice-thickness nudging, we ultimately complete the spin-up procedure with thermally and dynamically evolved, high-resolution ice-sheet simulations with ice thicknesses and bed geometries that are close to observed values (Extended Data Figs 7 and 8). Despite the broad agreement between modelled and observed values, there remain areas of mismatch, owing to the 140 years of unconstrained evolution from 1860 to 2000. In Antarctica, one important area of mismatch is in the Amundsen Sea, where our simulation is thinner than observed, has slower-than-observed velocities in Pine Island Glacier and has faster-than-observed velocities in Thwaites Glacier. Although all of our sea-level-equivalent volume calculations are bias-corrected using a control run that also uses this initial state, we cannot rule out the possibility that modelled dynamics might differ if our present-day state were closer to observed values. It is not certain, however, that our initial state would necessarily promote grounding-line retreat, because experiments forced with regional climate and ocean model outputs led to a stabilization, or even advance, of the grounding line in this sector (see below). There is clearly a threshold in this sector that makes the ice-sheet margin especially sensitive to ocean thermal forcing.

From these spun up Greenland and Antarctic ice-sheet models, we run forward experiments from 1860 to 2100 using full model physics and the CMIP5 climatologies described above for RCP4.5 and RCP8.5. Although our ice sheets are well evolved, it is essential that they also correctly reproduce observed trends in recent mass changes. To that end, we undertake a manual procedure in which our simulations are repeatedly run at the full desired resolution (2.5 km and 5 km) but with different parameterizations. Although other studies have very effectively used an ensemble approach[17,20], in which multiple parameter combinations are imposed and model validation is conducted on the final body of outputs, this would be computationally prohibitive for the high-resolution simulations described here. Instead, we analyse each model run in turn, and make parameter adjustments on the basis of the nature of any observed mismatch with empirical data. This approach results in simulations that fit multiple parameters not just at a single point in time, but over the periods of time for which observational constraints exist (Fig. 1). Our tuning procedure for Greenland uses adjustments to surface mass balance and to basal sliding parameters to fit our simulations to observed trends. Our surface mass balance adjustment is based on previous studies (see main text), as is our basal sliding refinement. With the latter, however, we recognize that our approach is just one of the ways in which a fit to constraints might be achieved. Sensitivity tests illustrate the effect of applying a steeper sliding reduction, or none at all (Extended Data Fig. 5d). Where no tapered reduction in basal traction is applied, net mass balance declines slightly (owing to the reduction in refreezing), but is far too high to agree with observations (Extended Data Fig. 5d, orange line). Doubling the reduction in basal traction used in our optimized scenario (blue line) results in a net mass balance trajectory that is only just in agreement with the observations, if published uncertainties are considered (Extended Data Fig. 5d, light blue line). Rates of mass loss at 2100 are around 33% lower than the optimized scenario in the 'No taper' experiment and 33% higher in the 'Steep taper' experiment. Future changes in basal sliding cannot be known, so we are not able to fully constrain mass loss rates that arise from dynamic processes such as these; this leads to uncertainty in our results. Because dynamic thinning is fundamentally self-limiting[43,44] (by encouraging marine-terminating ice-sheet margins to retreat onto land, where they tend to stabilize), our approach—targeting a central fit to the observational data—should reduce the errors in our projections as far as is possible; however, we cannot rule out the possibility that mass loss rates by 2100 may be higher or lower than we predict. Higher-resolution simulations than ours[84] may better resolve smaller outlet glaciers and thus perform better in this regard.

Once tuned in this manner, we begin the following experimental procedure. We do not use fully coupled models. Instead, we run a suite of ice-sheet simulations under the two RCP scenarios and three stabilization scenarios described above. These simulations reveal the differences between emissions scenarios and stabilization times (Extended Data Fig. 4), but do not incorporate ice–ocean–atmosphere feedbacks. To gauge the importance of these feedbacks we undertake additional ice-sheet simulations for RCP4.5 and RCP8.5. To do this, we add meltwater fluxes from the first iteration of our two ice sheets as a surface freshwater flux to the oceans around the two ice sheets across a region adjacent to where the ice is lost (see Methods section 'Climate and ocean model' section for definition of mask areas). For this we use the LOVECLIM intermediate-complexity climate model. The LOVECLIM simulations from 2000 to 2100 evolve from a present-day equilibrium state and are perturbed only by the addition of meltwater. Thus, the differences in these simulations, compared to a control run in which no meltwater is added, are a direct consequence of the meltwater forcing. Although this approach is simple, the consequences of adding the freshwater flux in our model are qualitatively similar to those produced with more sophisticated ocean models that allow melt input at depth[85,86]: vertical mixing is reduced, leading to surface cooling and an associated expansion of sea ice. The depth at which meltwater is released appears to have little impact on modelled sea-ice response[85]. However, we recognize that the approximations inherent in this approach may mean that we do not fully resolve many of the finer-scale aspects of the oceanic response. Over

seasonal to multi-annual timescales, for example, fluctuations in the depth of the thermocline (which separates colder surface water from warmer subsurface water) occur[87–89]. These changes are driven by local oceanic and atmospheric conditions and are also known to influence basal melt rates, but currently only high-resolution limited-domain ocean or coupled ocean–ice-sheet models are able to capture such effects[45,88]. Similarly, our coarse-resolution ocean model most probably underrepresents advective heat transfer by mesoscale eddies[90,91], which are critical in transferring energy from the open ocean into continental shelf embayments such as the Weddell and Ross seas.

Acknowledging these simplifications, we take the outputs from our meltwater-perturbed climate model simulations and repeat our ice-sheet simulations from 2000 to 2100, but add the air temperature, precipitation and ocean temperature anomalies to our original CMIP5 climate forcings. This iteration aims to capture the influence of ice–ocean–atmosphere feedbacks on the ice sheet. The results of these simulations are shown in Fig. 3. Because the meltwater feedback results in additional loss of ice from the two ice sheets, arising primarily from subsurface ocean warming, we re-run our LOVECLIM experiments for a second time but update the meltwater forcing to include the slight increase from the second ice-sheet run. The 30-year-averaged climate anomalies that arise from this second iteration of the climate model are shown in Fig. 4. Additional iterations of this process, or a tighter temporal coupling, might further refine the emergent climate anomalies by allowing feedback mechanisms (positive and negative) to occur more quickly, but are computationally more demanding. To estimate meltwater-induced changes in climate variability, we calculate the standard deviation of climate fields from the de-trended meltwater-forced runs and subtract the initial conditions from the century-end values. By then removing any background trend (calculated from our unforced control experiment), we derive a measure of how much our meltwater fluxes affect climate variability by the end of the century, compared to simulations in which such fluxes are omitted.

We also investigated the possible effect of driving our Antarctic Ice Sheet model with high-resolution regional climate[49] and ocean[71,92] model outputs, which directly provide melt fields for upper and lower ice-sheet boundaries, respectively. Compared to our RCP8.5 simulation using the CMIP5 climatology, our experiment forced with these regional models showed lower mass loss by 2100, and grounding-line advance of Amundsen Sea glaciers. This is not consistent with observational constraints, and probably arises from the fact that although the ice-sheet model geometry is free to evolve neither of the regional models used as inputs included an evolving ice-sheet mask. Consequently, effects such as increased surface melt due to surface lowering (the elevation–melt feedback) are not captured, allowing the glacier margin to thicken and stabilize over time and thus reducing the influence of oceanic melt. This result highlights the need for future regional modelling studies to incorporate evolving ice-sheet geometries wherever possible.

For our sea-level calculations, we add the geometries of our two ice sheets at 5-year intervals from the second iteration of the ice-sheet model to our sea-level model. The sea-level model includes Earth rotation and deformation of a radially varying viscoelastic Earth model and predicts a time-evolving gravitationally self-consistent spatial pattern of sea-level change during the twenty-first century. We run experiments in which we calculate the global fingerprints that arise from ice-sheet mass loss from each ice sheet individually and combined. Outputs are scaled to the global-mean sea-level equivalent derived from our ice-sheet model (Fig. 2d). The result of the combined ice-sheet simulation is shown in Fig. 4d. Although the global sea-level model produces a self-consistent pattern of sea-level rise, it does not capture the regional changes in sea surface height that arise from differential expansion of the water column due to oceanic temperature changes. Adding the sea surface height anomaly (perturbed minus control experiment) from our climate simulations to our global sea-level simulation yields a more complex pattern of sea-level rise that differs primarily in the Southern Ocean, where subsurface ocean warming is greatest (Fig. 4h).

Code availability. PISM is freely available as open-source code from https://github.com/pism/pism.git. LOVECLIM is freely available for download from https://www.elic.ucl.ac.be/modx/index.php?id=81. Figures were generated using Generic Mapping Tools[93]. Most figures use perceptually uniform colour palettes from the Scientific Colour Maps collection[94] and the CET Perceptually Uniform Colour Maps[95].

Data availability

CMIP5 data were downloaded from http://climexp.knmi.nl/. Antarctic bedrock topography and ice thickness data are from the BEDMAP2 compilation, available at https://secure.antarctica.ac.uk/data/bedmap2/. Greenland topography and ice thickness data are from BedMachine v3, available at https://nsidc.org/data/idbmg4. Greenland mass balance and geothermal heat flux data are available from the seaRISE website: http://websrv.cs.umt.edu/isis/index.php/Data. Information on Antarctic surface mass balance data are available at http://www.projects.science.uu.nl/iceclimate/models/antarctica.php#racmo23. Antarctic geothermal heat flux data are available at https://doi.pangaea.de/10.1594/PANGAEA.882503. Drainage basin outlines as shown in Fig. 3 are based on ICESat data[96]. Antarctic grounding lines and calving lines shown in Fig. 3a are from the MODIS-MOA 2009 dataset[97,98]. The datasets generated and analysed during this study are also available from the corresponding author on reasonable request.

51. Winkelmann, R. et al. The Potsdam Parallel Ice Sheet Model (PISM-PIK) – part 1: model description. *Cryosphere* **5**, 715–726 (2011).
52. Aschwanden, A., Bueler, E., Khroulev, C. & Blatter, H. An enthalpy formulation for glaciers and ice sheets. *J. Glaciol.* **58**, 441–457 (2012).
53. Feldmann, J., Albrecht, T., Khroulev, C., Pattyn, F. & Levermann, A. Resolution-dependent performance of grounding line motion in a shallow model compared to a full-Stokes model according to the MISMIP3d intercomparison. *J. Glaciol.* **60**, 353–360 (2014).
54. Golledge, N. R. et al. Antarctic climate and ice sheet configuration during a peak-warmth early Pliocene interglacial. *Clim. Past* **13**, 959–975 (2017).
55. Seroussi, H. & Morlighem, M. Representation of basal melting at the grounding line in ice flow models. *Cryosphere* **12**, 3085–3096 (2018).
56. Milillo, P. et al. On the short-term grounding zone dynamics of Pine Island Glacier, West Antarctica, observed with COSMO-SkyMed interferometric data. *Geophys. Res. Lett.* **44**, 10436–10444 (2017).
57. van den Broeke, M., Bus, C., Ettema, J. & Smeets, P. Temperature thresholds for degree-day modelling of Greenland ice sheet melt rates. *Geophys. Res. Lett.* **37**, L18501 (2010).
58. Hellmer, H. & Olbers, D. A two-dimensional model for the thermohaline circulation under an ice shelf. *Antarct. Sci.* **1**, 325–336 (1989).
59. Rignot, E. & Jacobs, S. S. Rapid bottom melting widespread near Antarctic Ice Sheet grounding lines. *Science* **296**, 2020–2023 (2002).
60. Hellmer, H., Kauker, F., Timmermann, R., Determann, J. & Rae, J. Twenty-first-century warming of a large Antarctic ice-shelf cavity by a redirected coastal current. *Nature* **485**, 225–228 (2012).
61. Levermann, A. et al. Kinematic first-order calving law implies potential for abrupt ice-shelf retreat. *Cryosphere* **6**, 273–286 (2012).
62. Fretwell, P. et al. Bedmap2: improved ice bed, surface and thickness datasets for Antarctica. *Cryosphere* **7**, 375–393 (2013).
63. Morlighem, M. et al. BedMachine v3: complete bed topography and ocean bathymetry mapping of Greenland from multibeam echo sounding combined with mass conservation. *Geophys. Res. Lett.* **44**, 11051–11061 (2017).
64. Van Wessem, J. et al. Improved representation of East Antarctic surface mass balance in a regional atmospheric climate model. *J. Glaciol.* **60**, 761–770 (2014).
65. Ettema, J. et al. Higher surface mass balance of the Greenland ice sheet revealed by high-resolution climate modeling. *Geophys. Res. Lett.* **36**, L12501 (2009).
66. Martos, Y. M. et al. Heat flux distribution of Antarctica unveiled. *Geophys. Res. Lett.* **44**, 11417–11426 (2017).
67. Shapiro, N. & Ritzwoller, M. Inferring surface heat flux distributions guided by a global seismic model: particular application to Antarctica. *Earth Planet. Sci. Lett.* **223**, 213–224 (2004).
68. Sallée, J.-B. et al. Assessment of Southern Ocean water mass circulation and characteristics in CMIP5 models: historical bias and forcing response. *J. Geophys. Res.* **118**, 1830–1844 (2013).
69. Turner, J., Bracegirdle, T. J., Phillips, T., Marshall, G. J. & Hosking, J. S. An initial assessment of Antarctic sea ice extent in the CMIP5 models. *J. Clim.* **26**, 1473–1484 (2013).
70. Bracegirdle, T. J. et al. Assessment of surface winds over the Atlantic, Indian, and Pacific Ocean sectors of the Southern Ocean in CMIP5 models: historical bias, forcing response, and state dependence. *J. Geophys. Res.* **118**, 547–562 (2013).
71. Naughten, K. A. et al. Future projections of Antarctic ice shelf melting based on CMIP5 scenarios. *J. Clim.* **31**, 5243–5261 (2018).
72. Goosse, H. et al. Description of the Earth system model of intermediate complexity LOVECLIM version 1.2. *Geosci. Model Dev.* **3**, 603–633 (2010).
73. Gent, P. R. & McWilliams, J. C. Isopycnal mixing in ocean circulation models. *J. Phys. Oceanogr.* **20**, 150–155 (1990).
74. Menviel, L., Timmermann, A., Timm, O. E. & Mouchet, A. Deconstructing the Last Glacial termination: the role of millennial and orbital-scale forcings. *Quat. Sci. Rev.* **30**, 1155–1172 (2011).
75. Abram, N. J. et al. Early onset of industrial-era warming across the oceans and continents. *Nature* **536**, 411–418 (2016).
76. Menviel, L. et al. Southern Hemisphere westerlies as a driver of the early deglacial atmospheric CO_2 rise. *Nat. Commun.* **9**, 2503 (2018).
77. Randall, D. A. et al. in *Climate Change 2007: The Physical Science Basis. Contribution of Working Group I to the Fourth Assessment Report of the Intergovernmental Panel on Climate Change* (eds Solomon, S. et al.) 589–662 (Cambridge Univ. Press, Cambridge, 2007).
78. Gomez, N., Mitrovica, J. X., Huybers, P. & Clark, P. U. Sea level as a stabilizing factor for marine-ice-sheet grounding lines. *Nat. Geosci.* **3**, 850–853 (2010).
79. Dziewonski, A. M. & Anderson, D. L. Preliminary reference Earth model. *Phys. Earth Planet. Inter.* **25**, 297–356 (1981).
80. Lambeck, K., Smither, C. & Ekman, M. Tests of glacial rebound models for Fennoscandinavia based on instrumented sea- and lake-level records. *Geophys. J. Int.* **135**, 375–387 (1998).

81. Mitrovica, J. X. & Forte, A. M. A new inference of mantle viscosity based upon joint inversion of convection and glacial isostatic adjustment data. *Earth Planet. Sci. Lett.* **225**, 177–189 (2004).
82. Lambeck, K., Rouby, H., Purcell, A., Sun, Y. & Sambridge, M. Sea level and global ice volumes from the Last Glacial Maximum to the Holocene. *Proc. Natl Acad. Sci. USA* **111**, 15296–15303 (2014).
83. Stuhne, G. & Peltier, W. Reconciling the ICE-6G_C reconstruction of glacial chronology with ice sheet dynamics: the cases of Greenland and Antarctica. *J. Geophys. Res.* **120**, 1841–1865 (2015).
84. Aschwanden, A., Fahnestock, M. A. & Truffer, M. Complex Greenland outlet glacier flow captured. *Nat. Commun.* **7**, 10524 (2016).
85. Pauling, A. G., Bitz, C. M., Smith, I. J. & Langhorne, P. J. The response of the Southern Ocean and Antarctic sea ice to freshwater from ice shelves in an Earth system model. *J. Clim.* **29**, 1655–1672 (2016).
86. Merino, N. et al. Impact of increasing Antarctic glacial freshwater release on regional sea-ice cover in the Southern Ocean. *Ocean Model.* **121**, 76–89 (2018).
87. Dong, S., Sprintall, J., Gille, S. T. & Talley, L. Southern Ocean mixed-layer depth from Argo float profiles. *J. Geophys. Res.* **113**, C06013 (2008).
88. Dutrieux, P. et al. Strong sensitivity of Pine Island ice-shelf melting to climatic variability. *Science* **343**, 174–178 (2014).
89. Webber, B. G. et al. Mechanisms driving variability in the ocean forcing of Pine Island Glacier. *Nat. Commun.* **8**, 14507 (2017).
90. Thompson, A. F., Heywood, K. J., Schmidtko, S. & Stewart, A. L. Eddy transport as a key component of the Antarctic overturning circulation. *Nat. Geosci.* **7**, 879–884 (2014).
91. Stewart, A. L. & Thompson, A. F. Eddy-mediated transport of warm Circumpolar Deep Water across the Antarctic Shelf Break. *Geophys. Res. Lett.* **42**, 432–440 (2015).
92. Naughten, K. A. et al. Intercomparison of Antarctic ice-shelf, ocean, and sea-ice interactions simulated by MetROMS-iceshelf and FESOM 1.4. *Geosci. Model Dev.* **11**, 1257–1292 (2018).
93. Wessel, P., Smith, W. H., Scharroo, R., Luis, J. & Wobbe, F. Generic mapping tools: improved version released. *Eos* **94**, 409–410 (2013).
94. Crameri, F. Geodynamic diagnostics, scientific visualisation and StagLab 3.0. *Geosci. Model Dev.* **11**, 2541–2562 (2018).
95. Kovesi, P. Good colour maps: how to design them. *Preprint at* https://arxiv.org/abs/1509.03700 (2015).
96. Zwally, H. J., Giovinetto, M. B., Beckley, M. A. & Saba, J. L. Antarctic and Greenland Drainage Systems. *GSFC Cryospheric Sciences Laboratory* http://icesat4.gsfc.nasa.gov/cryo_data/ant_grn_drainage_systems.php (2012).
97. Scambos, T. A., Haran, T. M., Fahnestock, M. A., Painter, T. H. & Bohlander, J. Modis-based Mosaic of Antarctica (MOA) data sets: continent-wide surface morphology and snow grain size. *Remote Sens. Environ.* **111**, 242–257 (2007).
98. Haran, T., Bohlander, J., Scambos, T., Painter, T., and Fahnestock, M. MODIS Mosaic of Antarctica 2008–2009 (MOA2009) Image Map. *National Snow and Ice Data Center* https://doi.org/10.7265/N5KP8037 (2014).
99. Rignot, E., Jacobs, S., Mouginot, J. & Scheuchl, B. Ice-shelf melting around Antarctica. *Science* **341**, 266–270 (2013).
100. Depoorter, M. A. et al. Calving fluxes and basal melt rates of Antarctic ice shelves. *Nature* **502**, 89–92 (2013).
101. Nagler, T., Rott, H., Hetzenecker, M., Wuite, J. & Potin, P. The Sentinel-1 mission: new opportunities for ice sheet observations. *Remote Sens.* **7**, 9371–9389 (2015).
102. Rignot, E., Mouginot, J. & Scheuchl, B. Ice flow of the Antarctic Ice Sheet. *Science* **333**, 1427–1430 (2011).
103. Rignot, E. et al. Recent Antarctic ice mass loss from radar interferometry and regional climate modelling. *Nat. Geosci.* **1**, 106–110 (2008).
104. King, M. A. et al. Lower satellite-gravimetry estimates of Antarctic sea-level contribution. *Nature* **491**, 586–589 (2012).
105. Helm, V., Humbert, A. & Miller, H. Elevation and elevation change of Greenland and Antarctica derived from CryoSat-2. *Cryosphere* **8**, 1539–1559 (2014).
106. Martín-Español, A. et al. Spatial and temporal Antarctic Ice Sheet mass trends, glacio-isostatic adjustment, and surface processes from a joint inversion of satellite altimeter, gravity, and GPS data. *J. Geophys. Res.* **121**, 182–200 (2016).
107. Gardner, A. S. et al. Increased West Antarctic and unchanged East Antarctic ice discharge over the last 7 years. *Cryosphere* **12**, 521–547 (2018).
108. McMillan, M. et al. Increased ice losses from Antarctica detected by CryoSat-2. *Geophys. Res. Lett.* **41**, 3899–3905 (2014).
109. Velicogna, I. & Wahr, J. Time-variable gravity observations of ice sheet mass balance: Precision and limitations of the GRACE satellite data. *Geophys. Res. Lett.* **40**, 3055–3063 (2013).
110. Lenaerts, J., van den Broeke, M., van de Berg, W., van Meijgaard, E. & Munneke, P. A new, high-resolution surface mass balance map of Antarctica (1979–2010) based on regional atmospheric climate modeling. *Geophys. Res. Lett.* **39**, L04501 (2012).
111. Turner, J., Connolley, W. M., Leonard, S., Marshall, G. J. & Vaughan, D. G. Spatial and temporal variability of net snow accumulation over the Antarctic from ECMWF re-analysis project data. *Int. J. Climatol.* **19**, 697–724 (1999).
112. van de Berg, W. J., van den Broeke, M. R., Reijmer, C. H. & van Meijgaard, E. Reassessment of the Antarctic surface mass balance using calibrated output of a regional atmospheric climate model. *J. Geophys. Res.* **111**, D11104 (2006).
113. Liu, Y. et al. Ocean-driven thinning enhances iceberg calving and retreat of Antarctic ice shelves. *Proc. Natl Acad. Sci. USA* **112**, 3263–3268 (2015).
114. Rignot, E., Box, J. E., Burgess, E. & Hanna, E. Mass balance of the Greenland ice sheet from 1958 to 2007. *Geophys. Res. Lett.* **35**, L20502 (2008).
115. Shepherd, A. et al. A reconciled estimate of ice-sheet mass balance. *Science* **338**, 1183–1189 (2012).
116. Rignot, E. & Kanagaratnam, P. Changes in the velocity structure of the Greenland ice sheet. *Science* **311**, 986–990 (2006).
117. Sasgen, I. et al. Timing and origin of recent regional ice-mass loss in Greenland. *Earth Planet. Sci. Lett.* **333–334**, 293–303 (2012).
118. Box, J. E., Bromwich, D. H. & Bai, L. S. Greenland ice sheet surface mass balance 1991–2000: application of polar MM5 mesoscale model and in situ data. *J. Geophys. Res.* **109**, D16105 (2004).
119. Wilson, N. J., Straneo, F. & Heimbach, P. Satellite-derived submarine melt rates and mass balance (2011–2015) for Greenland's largest remaining ice tongues. *Cryosphere* **11**, 2773–2782 (2017).
120. Bigg, G. R. et al. A century of variation in the dependence of Greenland iceberg calving on ice sheet surface mass balance and regional climate change. *Proc. R. Soc. Lond. A* **470**, 20130662 (2014).

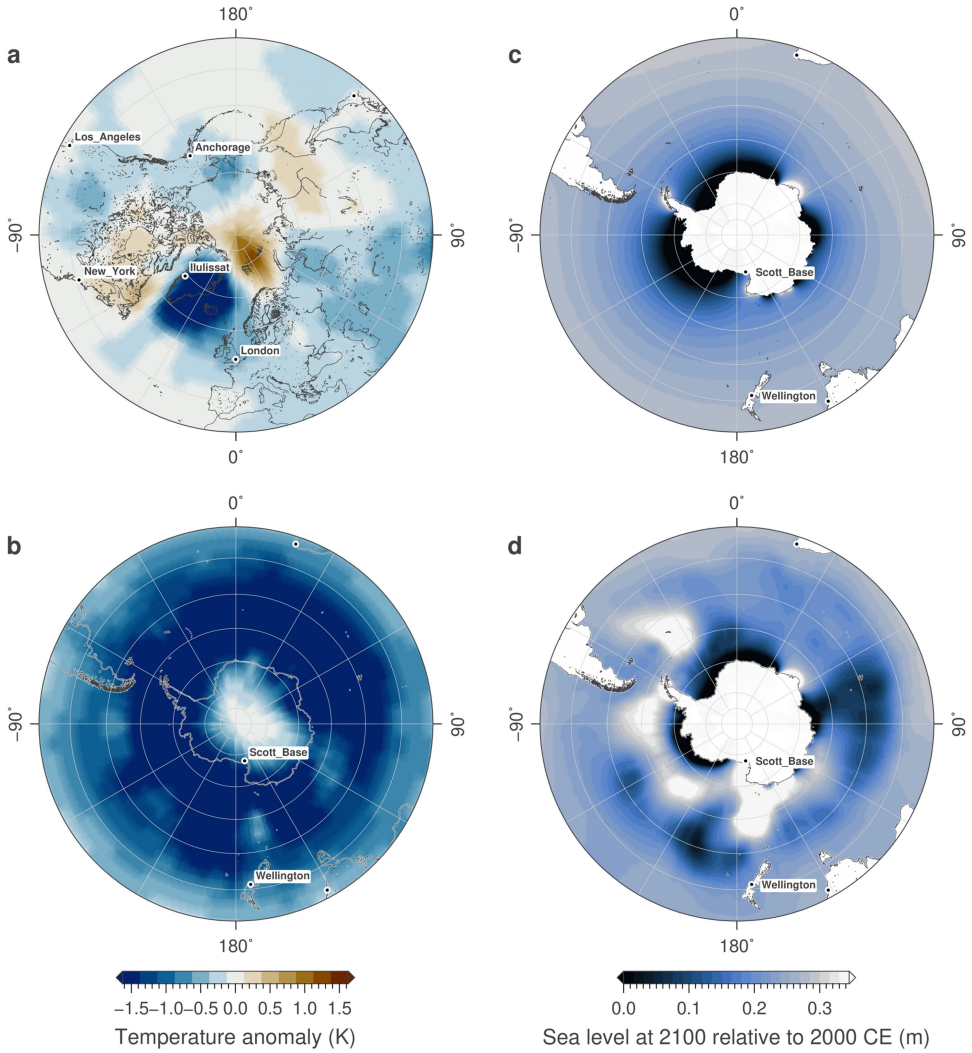

Extended Data Fig. 1 | High-latitude air temperature and sea-level anomalies. a, **b**, Air (surface) temperature anomalies at 2100 arising from meltwater perturbations from ice sheets simulated under an RCP8.5 climate scenario. Arctic landmasses experience slight cool or warm anomalies, but temperatures over the Arctic ocean warm substantially in the region to the northeast of Greenland (around Svalbard), as far north as the North Pole (**a**). In the Southern Hemisphere, cooling of up to 3–4 °C occurs across the Southern Ocean and around the margins of Antarctica (**b**). Temperature anomalies are 30-year means to avoid aliasing short-term variability. **c**, **d**, Sea-level changes in the Southern Ocean and around Antarctica computed from the sea-level model (**c**), and with the addition of sea surface height changes due to ocean temperature changes (**d**). The thermosteric anomalies are from a 30-year mean to avoid aliasing short-term variability.

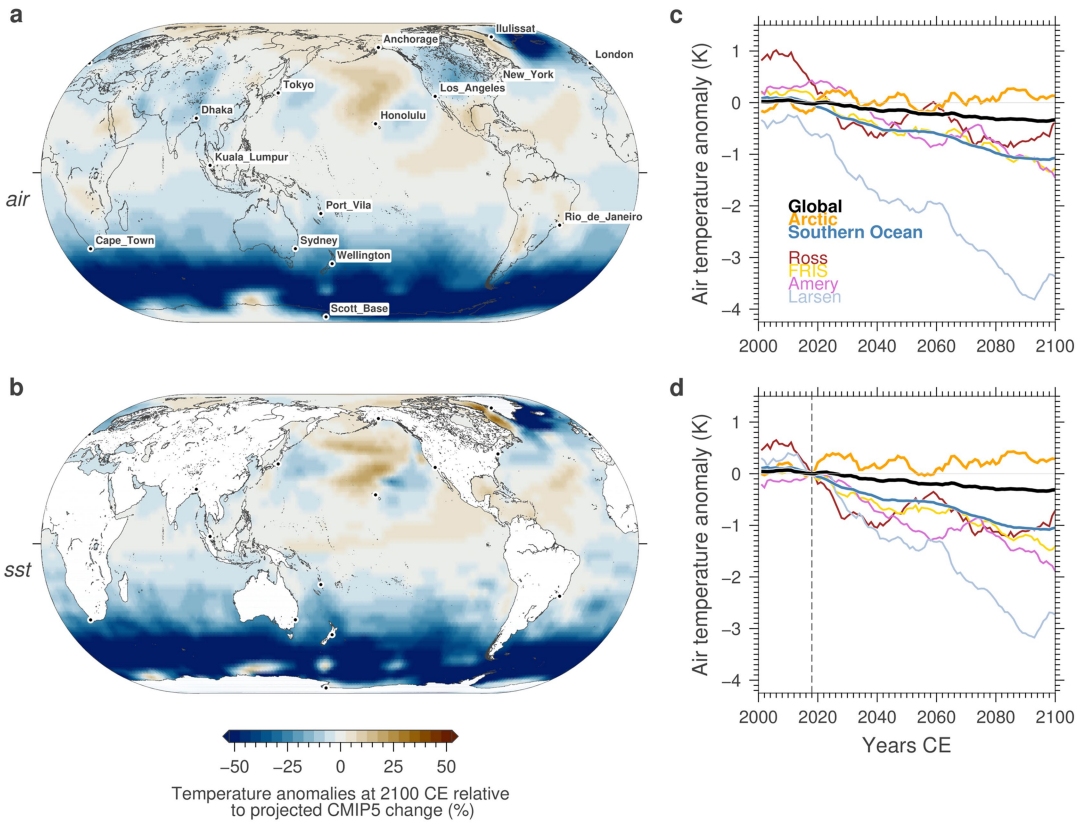

Extended Data Fig. 2 | Global and regional surface temperature anomalies. a, **b**, Surface air (**a**) and sea surface (**b**) temperature anomalies at 2100 arising solely from imposed meltwater fluxes, as a percentage of CMIP5 predictions based on emissions forcing but not including meltwater fluxes. **c**, Zonally and meridionally averaged surface air temperature anomalies for the globe, the Southern Ocean (40–85° S) and over the four largest ice shelves in Antarctica. **d**, Same as **c**, but adjusted to give changes relative to 2018.

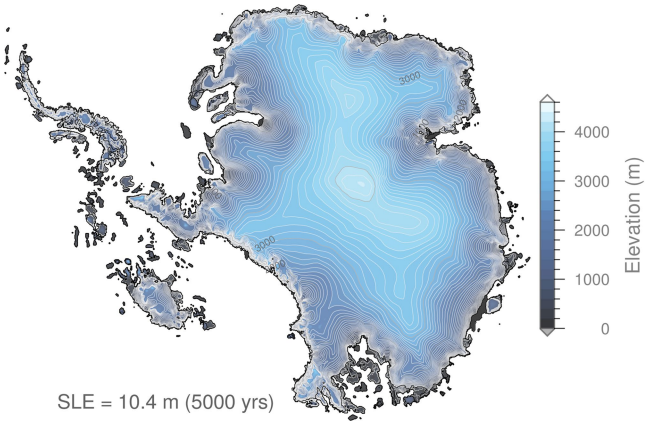

Extended Data Fig. 3 | Antarctic ice-sheet extent under Pliocene conditions. Shown are results of 5-km-resolution simulations of the Antarctic ice sheet under peak-warmth Pliocene conditions, based on proxy-constrained climate and ocean fields from regional climate modelling[54] but using an ice-sheet parameterization identical to that used for the RCP simulations presented in the main paper. The total sea-level-equivalent (SLE) mass loss after 5,000 years is 10.4 m, close to the 11.3 m simulated by a previous study that used ice-shelf hydrofracture and marine ice-cliff instability[20], neither of which are used here.

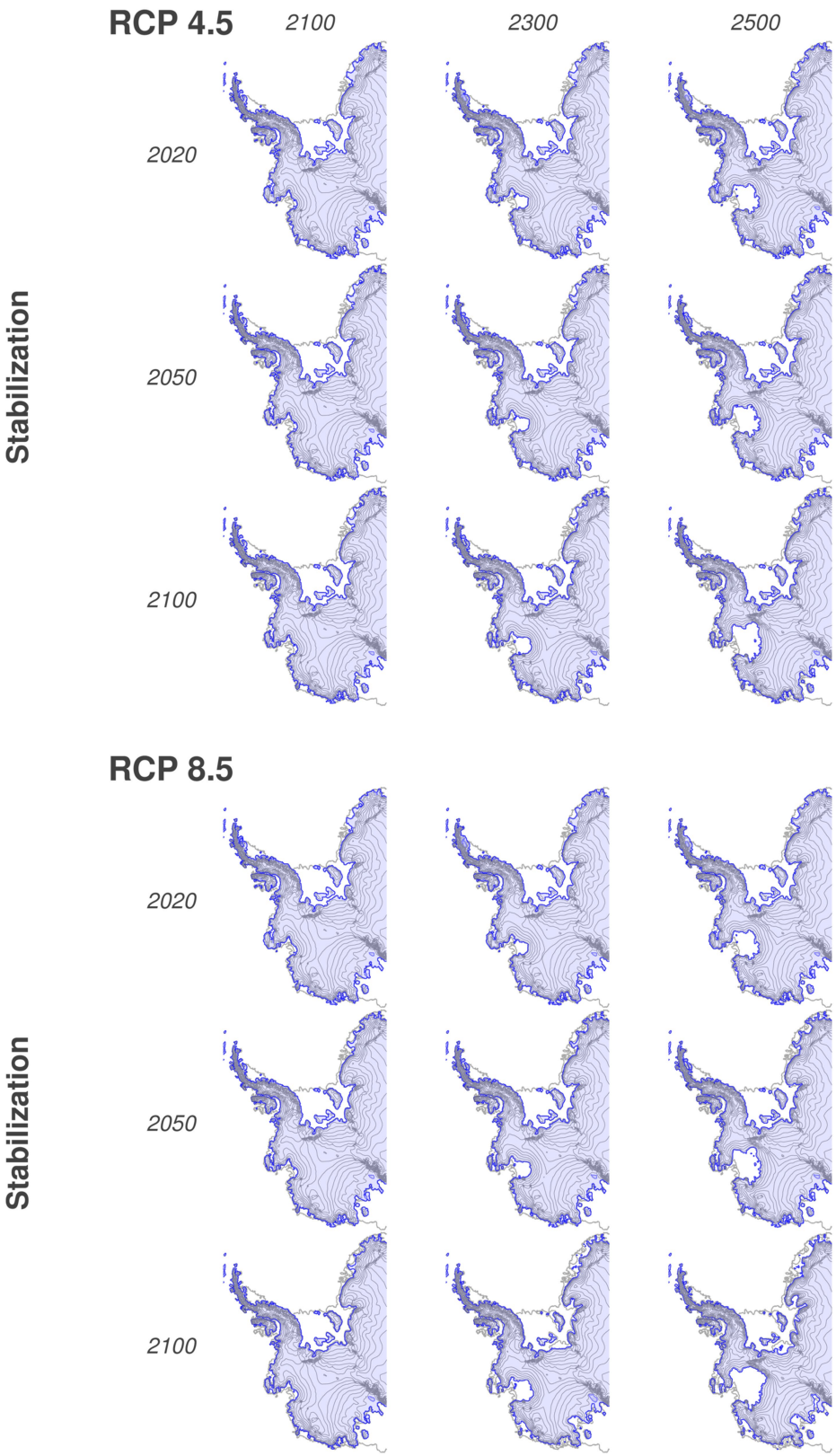

Extended Data Fig. 4 | Committed response of West Antarctica. The extent of grounded ice in West Antarctica at 2100, 2300 and 2500 is illustrated for two emissions pathways (RCP4.5 and RCP8.5) and for experiments in which the climate forcing is held constant from 2020, 2050 or 2100, but without the inclusion of ice–ocean–atmosphere feedbacks. Mass loss in these scenarios illustrates long-term commitments locked in by cumulative forcing up to the point of stabilization. Thwaites Glacier basin retreats in all scenarios, suggesting that the threshold for its stability has already been passed. Contour intervals are 250 m. Black lines show modern coast, for context.

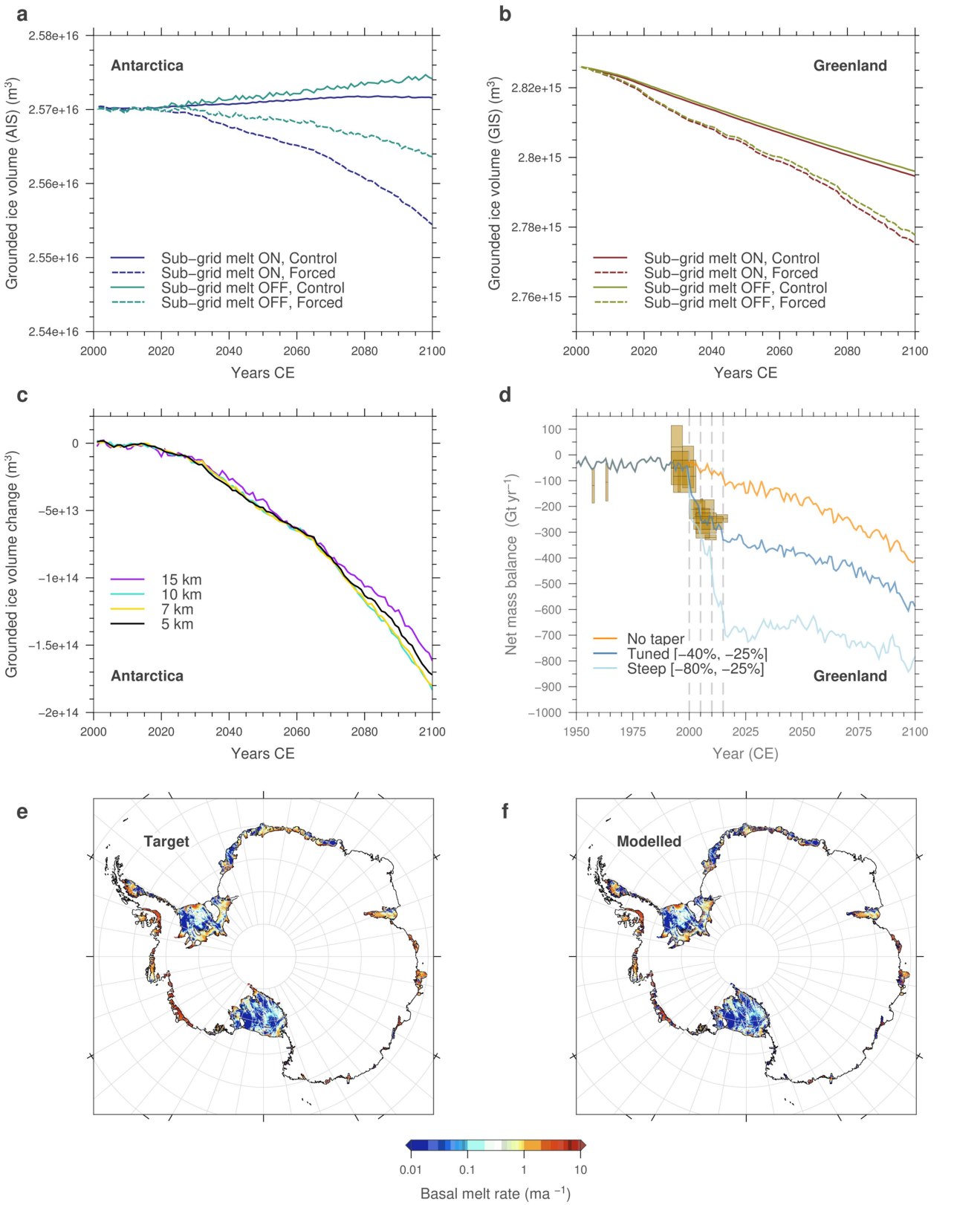

Extended Data Fig. 5 | See next page for caption.

Extended Data Fig. 5 | Grounding-line sensitivity and basal-melt parameterization . Control run (constant year-2000 climatology) and RCP8.5-forced experiments (including ice–ocean–atmosphere feedbacks) for Antarctica (**a**) and Greenland (**b**), with and without the incorporation of the sub-grid grounding-line melt scheme. Without the scheme, Antarctic ice volumes are higher in the forced run than with sub-grid melt enabled, but the control run also increases in volume, which suggests that other aspects of model parameterization would need to be optimized to ensure agreement with observational constraints (Extended Data Tables 1 and 2). Greenland simulations are far less affected by the sub-grid melt scheme. The Greenland runs shown all incorporate the evolving surface mass balance and basal traction parameterization (Methods), for clearer comparison between control and perturbed experiments. **c**, Change in grounded ice volume in Antarctica, compared to control runs, simulated by our ice-sheet model using a range of horizontal grid resolutions (see legend) but otherwise identical parameterization and including the sub-grid grounding-line basal melt scheme. **d**, Rate of Greenland Ice Sheet mass loss for the best-fitting simulation (dark blue line) compared to simulations in which either a steeper increase in sliding is applied (light blue line) or sliding is maintained at a constant value for the entire run (orange line). Numbers in brackets quantify the change in till friction angle in the piecewise-linear basal traction parameter below −200 m and above 500 m, relative to the 'No taper' experiment. Gold boxes show the time span (*x* axis) and uncertainty (*y* axis) of empirical data values used as targets during parameter optimization, from sources detailed in Extended Data Tables 1 and 2. **e**, **f**, Target melt rates from an empirically constrained[99,100] ice-sheet simulation[25] (**e**) are used as inputs to an inverse scheme that solves for a spatially distributed melt factor to translate CMIP5 sea surface temperatures into realistic melt fields (**f**). This approach greatly improves the representation of ice-shelf basal melting in our simulation compared to previous studies[18,20].

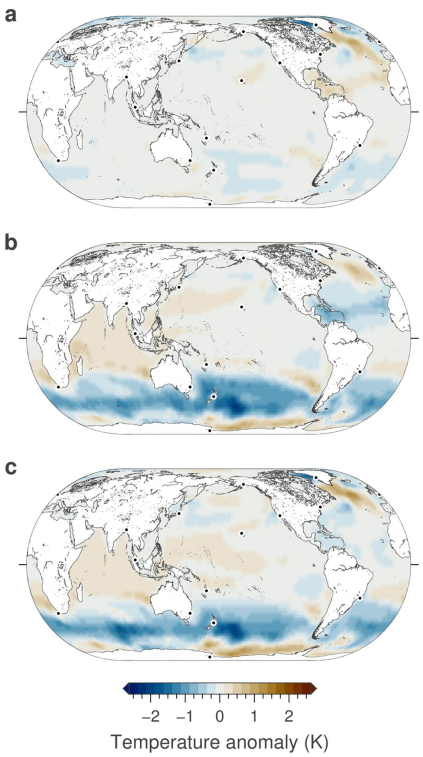

Extended Data Fig. 6 | Ice-sheet influence on subsurface ocean temperature. a–**c**, Ocean temperature anomalies by 2100 at 415-m depth from Greenland meltwater flux only (**a**), Antarctic meltwater flux only (**b**) and combined meltwater flux from both ice sheets (**c**). Anomalies are 30-year means to avoid aliasing short-term variability.

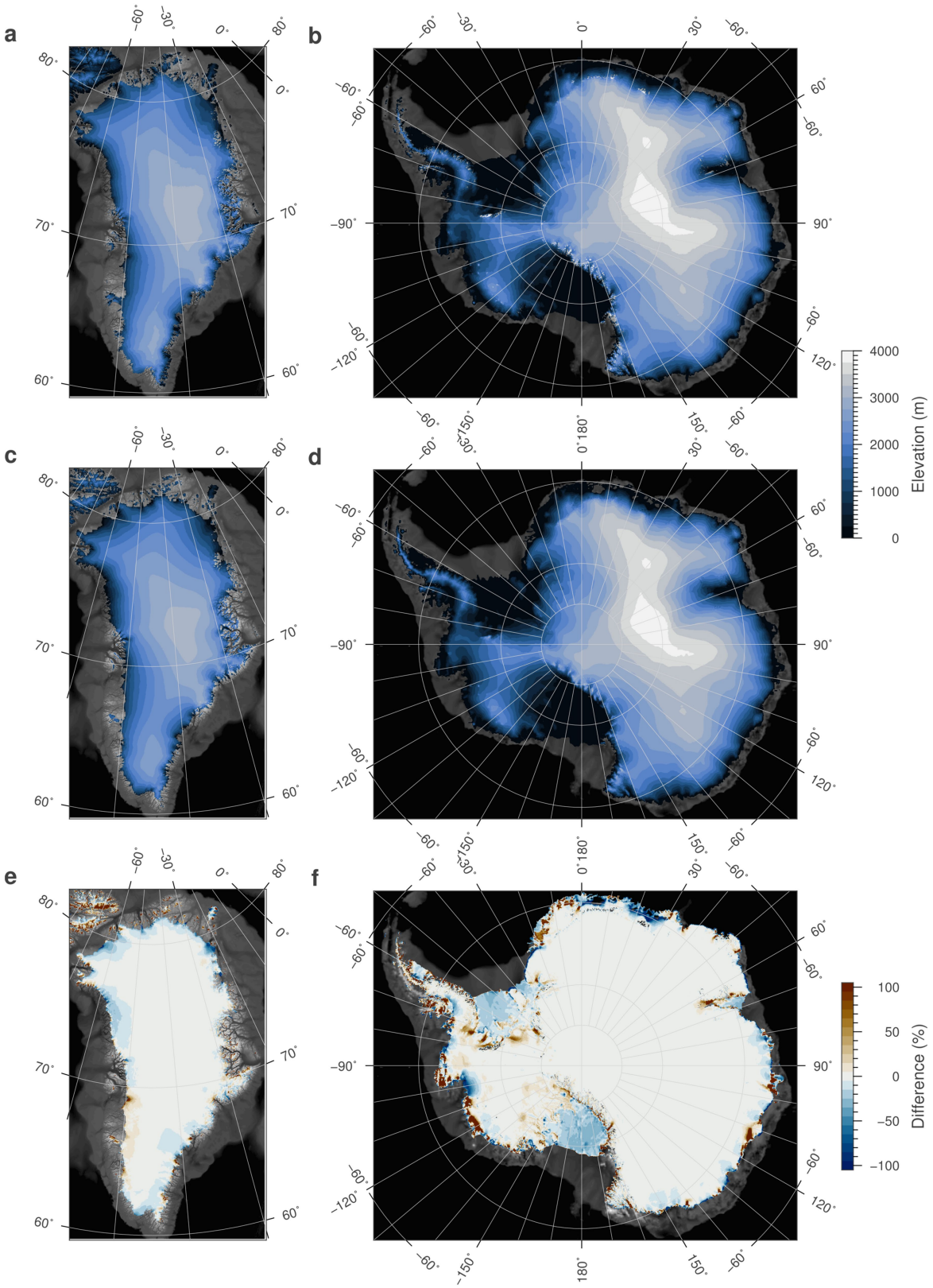

Extended Data Fig. 7 | Modelled versus measured surface elevation. a–d, Measured values of surface elevation of the Greenland[63] (**a**) and Antarctic[62] (**b**) ice sheets compared to modelled values (**c**, **d**) at year 2000. **e**, **f**, Differences between the two (modelled minus observed).

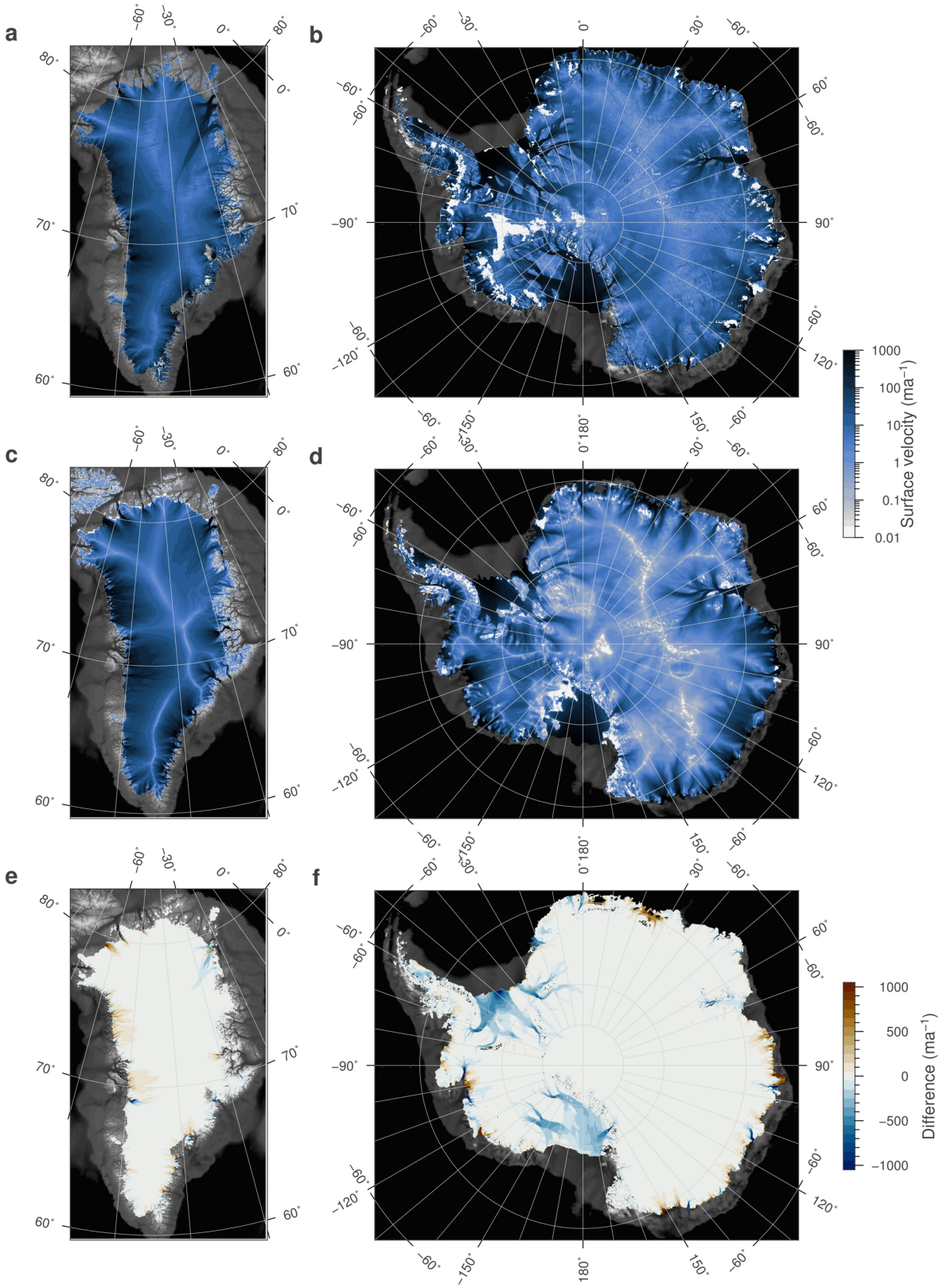

Extended Data Fig. 8 | Modelled versus measured surface velocity. a–d, Measured values of surface velocity of the Greenland[101] (**a**) and Antarctic[102] (**b**) ice sheets compared to modelled values (**c**, **d**) at year 2000. **e**, **f**, Differences between the two (modelled minus observed).

Extended Data Table 1 | Empirical constraints used to guide Antarctic Ice Sheet parameterization

Antarctica

		Period	Rate (Gt / yr)	Uncertainty (± Gt /yr)
Total mass	Bamber et al. (2018)	1992-1997	-27	106
		1997-2002	-103	106
		2002-2007	-25	54
		2007-2012	-117	28
		2012-2017	-191	47
	Gardner et al. (2018)	2008-2015	-183	94
	Shepherd et al. (2018)	1992-1997	-49	67
		1997-2002	-38	64
		2002-2007	-73	53
		2007-2012	-160	50
		2012-2017	-219	43
	Martin-Espanol et al. (2016)	2010-2013	-159	22
	Helm et al. (2014)	2011-2014	-116	76
	McMillan et al. (2014)	2010-2013	-159	48
	Velicogna & Wahr (2013)	2003-2011	-118	66
	King et al. (2012)	2002-2010	-69	18
	Rignot et al. (2008)	1995-1996	-112	91
		1999-2000	-138	92
		2005-2006	-196	92
SMB	Lenaerts et al. (2012)	1979-2010	2418	181
	Rignot et al. (2008)	1999-2000	2055	122
	van der Berg et al. (2006)	1980-2004	2521	33
	Turner et al. (1999)	1979-1993	2106	299
BMB	Liu et al. (2015)	2005-2011	1516	106
	Depoorter et al. (2013)	1995-2009	1454	174
	Rignot et al. (2013)	2003-2008	1325	235
Calving	Liu et al. (2015)	2005-2011	755	25
	Depoorter et al. (2013)	1995-2009	1321	144
	Rignot et al. (2013)	2003-2008	1089	139

Estimates of changes in total mass[1,5,103–109], surface mass balance (SMB)[103,110–112], sub-ice-shelf melt (BMB)[99,100,113] and iceberg calving[99,100,113] from recent satellite-based studies, including uncertainties. Data provide targets for ice-sheet simulations shown in Fig. 1.

Extended Data Table 2 | Empirical constraints used to guide Greenland Ice Sheet parameterization

Greenland

		Period	Rate (Gt / yr)	Uncertainty (± Gt /yr)
Total mass	Bamber et al. (2018)	1992-1997	31	83
		1997-2002	-47	81
		2002-2007	-206	28
		2007-2012	-320	10
		2012-2017	-247	15
	Forsberg et al. (2017)	2002-2015	-264	25
	Velicogna & Wahr (2013)	2003-2012	-265	40
	Sasgen et al. (2012)	2003-2009	-265	58
	Shepherd et al. (2012)	1992-2000	-51	65
		1993-2003	-83	63
		2000-2011	-211	37
	Rignot et al. (2008) GRL	1957-1958	-119	68
		1963-1964	-106	73
		1995-1996	-97	47
	Rignot & Kanagaratnam (2006)	2005-2006	-210	40
SMB	Rignot et al. (2008) GRL	1957-1958	272	41
		1963-1964	299	45
		1995-1996	300	45
		1999-2000	277	42
		2003-2004	242	36
		2004-2005	233	35
		2005-2006	234	35
		2006-2007	228	34
	Box & Bromwich (2004)	1992-1998	193	179.5
BMB	Wilson et al. (2017)	2011-2015	23.7	3.2
Calving	Bigg et al. (2014)	1900-1910	250	204
		1910-1920	216	185
		1920-1930	264	209
		1930-1940	267	172
		1940-1950	211	228
		1950-1960	148	187
		1960-1970	96	85
		1970-1980	254	340
		1980-1990	335	407
		1990-2000	659	345
		2000-2009	271	238

Estimates of changes in total mass[2,5,109,114–117], surface mass balance (SMB)[114,118], sub-ice-shelf melt (BMB)[119] and iceberg calving[120] from recent satellite-based and modelling studies, including uncertainties. Data provide targets for ice-sheet simulations shown in Fig. 1.